**Colorado
State**
University

ESSAYS ON RIVER MECHANICS

**Presented by the Graduate Students
in CE 717 - River Mechanics (Spring 1993)**

Instructor: P.Y. Julien

April, 1993

CER92-93-PYJ-5

Colorado State University

ESSAYS ON RIVER MECHANICS

Presented by the Graduate Students
in CE 717 - River Mechanics (Spring 1993)

Instructor: P.Y. Julien

April, 1993

CER92-93-PYJ-5

FOREWORD

I am very pleased to honor the work of the graduate students in the class CE 717-River Mechanics with this report of their technical papers. Each student worked on a particular aspect of river engineering in order to meet the following objectives:

1) familiarize with the recent literature and new methodologies not available in textbooks;
2) compare various methods (new versus old) and discuss the advancement of engineering technology on a given topic;
3) develop skills to point out the key elements of recent technological developments;
4) share interesting findings with the other students through an oral presentation and a written paper.

The requirements for this project were:

1) select a topic relevant to river mechanics and sediment transport;
2) conduct a literature review including papers published in the past five years;
3) compare new methods with those detailed in textbooks on either a theoretical basis or through comparison with an appropriate data set;
4) write a 15 page paper following the ASCE editorial standards (these papers are included herein).
5) discuss the major findings in a 30 minute oral presentation.

The reader will certainly agree with me that the objectives were met with great success. I am personally impressed with the overall quality of the reports presented and I can only compliment them on their effort.

Pierre Julien

Pierre Y. Julien
Associate Professor
Civil Engineering Department

TABLE OF CONTENTS

The Modified McNeil Sampler - A New Methodology For Armor Layer and Substrate Sampling

(Mitch Peters, Colorado State University, April 1993)

Abstract

This paper reviews several methods of sediment sampling, including the US BMH - 53, US BMH - 54, Hubbell sampler, and Freeze Core apparatus, and introduces the Modified McNeil sampler. The Modified McNeil sampler is explained, and its use is detailed. Benefits and drawbacks of this new sampling technique are discussed in light of the other sampling devices. Armor layer and substrate data taken from the Chama River, New Mexico, with the Hubbell, Freeze Core, and Modified McNeil samplers are summarized and compared. Statistically based methods for determining adequate sample size given particle sizes are also reviewed and presented.

1.1   Introduction:

The measurement of a stream's bed material is an elemental part of any analysis that is to be performed on that stream. Quantification of bed characteristics is important to determine hydraulic characteristics, stability in terms of sediment transport, and aquatic habitat. Due to the importance of bed material in understanding and predicting stream and wildlife response, many devices have been developed to measure this material. In the past, sophisticated mechanical devices like the BMH - 53 and BMH - 54 were used to measure bed material. More recently, samplers like the Hubbell, Freeze Core, and Modified McNeil, have been developed to provide a more representative sample of the river bed.

The Hubbell, Freeze Core, and Modified McNeil samplers have all been employed to sample the same reach of the Rio Chama in Northern New Mexico. In October, 1991 the Rio Chama was surveyed to assess the quality of spawning habitat, determine locations for bed sampling. The locations which met criteria of potential brown trout redd construction sites (depth between 3 and 18 inches, velocity of 0.2 to 0.4 feet per second) were sampled using the Hubbell and Freeze Core techniques at that

time. (3 Freeze Core and 2 Hubbell samples were taken at this site). Just over a year later, in January, 1993, the site closest to the dam was resampled using the Modified McNeil Sampler. Flow at this time was approximately 200 cfs. Results from the 1991 sampling are compared to
the 1992 results to check the validity of the Modified McNeil sampler.

Sample size is also determined for the material found at this location of the Chama River. The technique for determining sample size is presented and discussed. The actual size of the 1993 sample is compared to the determined statistical sample size, and further discussion of sample size feasibility is presented.
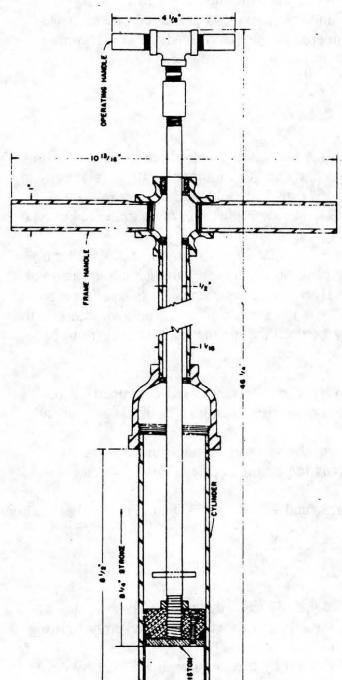
1.2   US BMH - 53, and US BMH - 54

"Bed material samplers, as first developed, may be divided into three types: The drag bucket, grab bucket, and vertical pipe". (Interagency Committee, 1940b). The vertical pipe type is represented by the US BMH -53, (see Figure 1), and the drag or grab bucket type is represented by the US BMH - 54 (see Figure 2). (The grab bucket type is essentially the same as the drag bucket type).

The US BMH - 53 is made up of a 9 inch (22.86 cm.) length of 2" (5.08 cm.) brass or Stainless steel pipe with a cutting edge on the bottom, and a suction piston at the top. As the sampler is driven into the river bed, the piston retracts creating a partial vacuum in the sampling chamber. This allows the sample to be withdrawn intact in the sampling chamber. This sampler can only be used in streams shallow enough to be waded. Advantages of this method include:

☐ The sampler is relatively light weight, compact, and self contained. This allows it to be easily transported to remote field locations by backpack, or raft, etc.
☐ If the sample can be removed from the sampler in small increments, its stratigraphy may be observed. This is important in determining fish and macroinvertebrate habitat.
☐ The sampler has few moving parts, and is most likely maintenance free - a big plus in the field.

Disadvantages of the BMH - 53 include:

■ The 2" (5.08 cm.) opening will obviously limit the samples largest clasts to 2" (5.08 cm.) round pieces. In most cobble bed streams this is a severely limiting factor.
■ The depth of the sample is also limited by the sampler to 8.5" (21.59 cm.). In some cases the material must be determined at greater depths than 8.5" (21.59 cm.).

FIG. 3.18.—US BMH-53 Bed Material Sampler

Figure 1

SECTION A-A

PLAN

ELEVATION

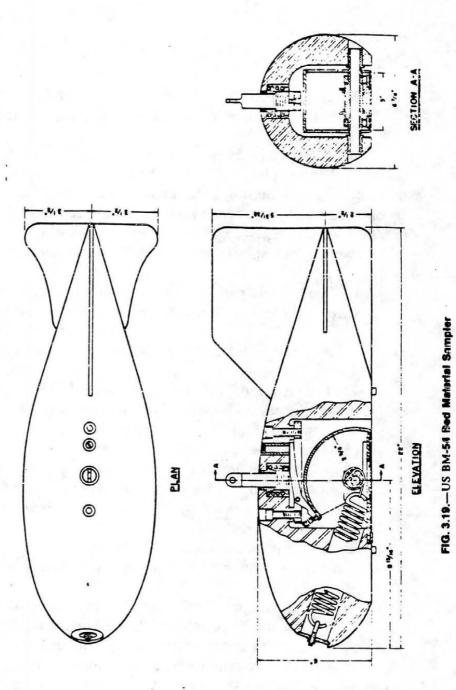FIG. 3.19.—US BM-54 Red Material Sampler

Figure 2

■ The sampler can only be used in wadeable streams. Again this limits sampling in deeper and faster running streams and rivers.

The US BMH - 54 is a 100 pound spring operated scoop drag/grab type bed sampler. The sampler is placed in the stream, and allowed to sink to the bottom. When it reaches the bed, tension is released on the suspension cable, and the spring operated scoop is released. The scoop rotates 180 degrees and takes a sample that is about 3" (7.62 cm.) wide and 2" (5.08 cm.) deep. The device is retrieved and the sample can be withdrawn. Advantages of the US BMH - 54 include:

☐ The sampler can be positioned with its suspension cable and therefore can be used in difficult to access areas with deep or fast water.

Disadvantages of the BMH - 54 include:

■ The weight of this device, 100 pounds, limits its applicability in areas which must be accessed by foot (far from vehicles).
■ Again the sample size is relatively small. The scoop allows a sample only 2" (5.08 cm.) deep and 3" (7.62 cm.) wide.
■ There are many moving parts involved in the operation of the trigger mechanism and the spring released spring. In the field these may become jammed, or obstructed by fine particles rendering the sampler useless, or causing down-time for repairs.
■ The upstream orientation of the mouth of the sampler may cause it to loose some fines in the operation of the scoop, and in dragging it to the surface.

"The drag and grab-bucket samplers are either too cumbersome to handle or do not obtain representative samples of the bed material. The vertical-pipe sampler is satisfactory for use in shallow streams". (Sedimentation Engineering, 1977). These samplers are relatively primitive, and have many drawbacks. As is mentioned in Sedimentation Engineering, 1977, they are for use in streams with bed material primarily made up of sand and gravel (not useful in situations with cobble or larger sized material).

1.3   Hubbell, and Freeze Core Samplers

Both the Hubbell, and the Freeze Core samplers were employed by the Bureau of Land Management in their 1991 measurement of Rio Chama bed material. At the location 1.2 miles downstream of El Vado Dam, 2 Hubbell samples were taken, along with 3 Freeze Cores. (This is the same location sampled in 1993 by Fish and Wildlife using the Modified McNeil method).

The Hubbell sampler (see Figure 3) is a dredge type sampler which is pulled across the channel bottom by a vehicle winch. The winch drags the Hubbell sampler, as field personnel guide it and maintain its position on the channel bed. The upper 10 to 15 cm. of bed material is sampled. (The width of the sampler opening is approximately 0.5 m.). Advantages of the Hubbell sampler include:

☐ The sampler opening (15 cm. by 50 cm.) is relatively large, it can sample material much larger than the BMH - 53 and BMH - 54.
☐ The sampler has no moving parts, and except reliance on a vehicle winch should be maintenance free.

Disadvantages of the Hubbell sampler include:

■ The 15 cm. by 50 cm. opening will still limit the sampling of large clasts. (Depending on their orientation as they enter the sampler opening).
■ The depth of the sample is again limited by the sampler to 15 cm.
■ The sampler can only be used in proximity to a winch equipped vehicle. This prohibits pack-in and raft-in utilization.
■ The sample collection bag will allow fines to flow through as the sampler is dragged across the channel bed.

The Freeze Core apparatus (see Figure 4) is an entirely different type of sampling device. It consists of three steel tipped pipes which are driven about 30 cm. into the channel bottom. After being placed, these pipes are injected with carbon dioxide gas under pressure. The pressurized gas serves to freeze the core of material immediately surrounding the pipes. (see Figure 5). This core is extracted from the channel with a winched cable attached to the tripod above the Freeze Core apparatus. Once extracted, the core is "defrosted" with a propane torch and separated into a spitter box (see also Figure 5). The spitter box allows the sample to be kept in 10 cm. intervals (0 - 10 cm., 10 - 20 cm., and 20 - 30 cm.). Advantages of the Freeze Core technique include:

☐ The core sample is not limited by a sampler opening, as in the other samplers discussed so far. This means that particle size sampled is not limited by sampler geometry, but rather it is limited by the capacity of the frozen core to hold the large pieces. (Results showed that particles larger than 64 mm., but not larger than 128 mm. were collected with this Freeze Core Apparatus).
☐ The sample may be analyzed stratigraphically while it is frozen, or in the thawed and separated condition. This adds important information when considering aquatic habitat.

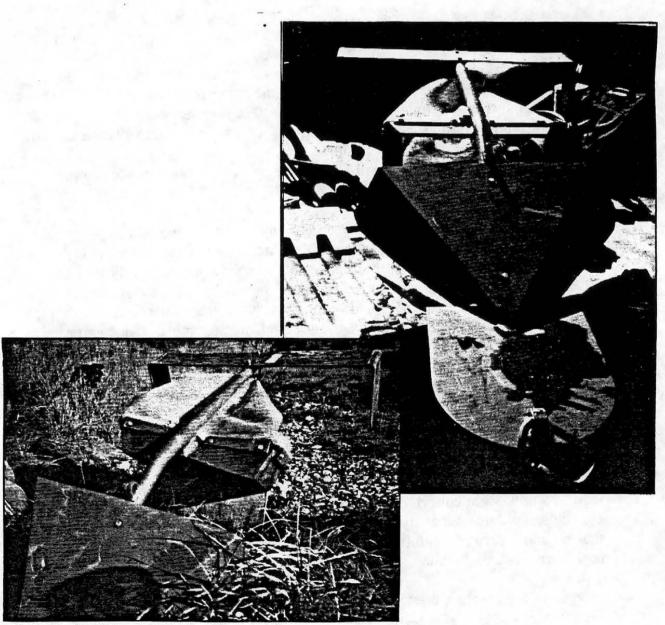Disadvantages of the Freeze Core technique include:

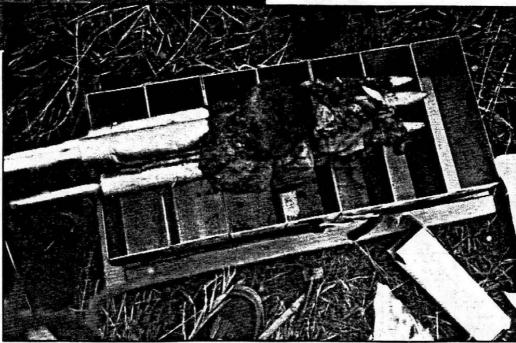**Figure 3** Hubbell sampler.

Figure 4

Figure 5 Freeze core apparatus.

■ The equipment used to obtain Freeze Core samples is fairly complex. One can (the size and weight of a SCUBA tank) of CO_2 is required for each sample. These tanks must be new, or if used, must be free from corrosion. If the CO_2 that is forced into the pipes is not pure, it will clog the jets. Once the jets are plugged, it takes at least an hour to clean them out.

■ The amount of equipment and CO_2 required, and dependence on a vehicle winch for sample extraction, restrict operations to vehicle access points. (Pack-in and raft-in use is not feasible).

■ Due to the complexity of the equipment, operation and maintenance can be quite time consuming.

■ The depth of the sample is limited by depth to which the pipes can be driven, in some stream conditions the pipes can be very difficult to drive..

1.4   Modified McNeil Sampler

The Modified McNeil sampler, a relatively new sampler, overcomes many of the drawbacks of the above mentioned samplers, and has many of its own strong-points. The Modified McNeil sampler (see Figure 6) is basically a 30 gallon drum with the bottom cut off. It ends up being about 30 inches tall and 20 inches in diameter (76.2 cm. tall by 50.8 cm. across). The cut end (sharp edge) of the drum is the end that goes
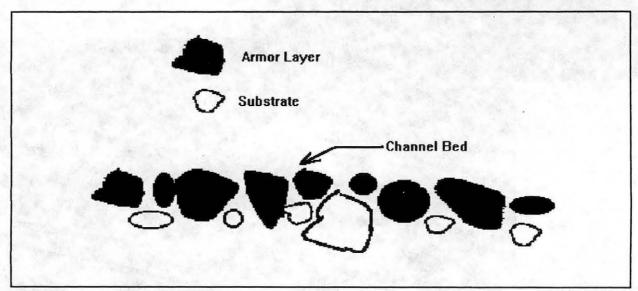

Figure 7

toward the channel bed, while the top of the drum has a slightly rolled edge, so that the operators don't get cut on it.

Samples are taken with the Modified McNeil sampler as follows: The sampler is

placed in the stream, and the armor layer is removed from within the barrel. For their purposes, the Fish and Wildlife people define the armor layer as anything exposed to the surface (see Figure 7). Clasts are removed to be kept with the sample if they are at least 50% within the sampler, they are discarded if they are more than 50% out of the sampler. Once the armor layer has been removed from the sampler at this location, the sampler is moved over, perpendicular to the flow direction (see Figure 8 below). The armor layer is removed, by hand (see Figure 9), at this sample station, and these steps are repeated until the armor layer has been removed from 5 or 6 stations. At the last station (the 5th or 6th station) the substrate is removed after the armor layer has been sampled. A small stainless steel bowl is used to scrape and remove the substrate from the bed
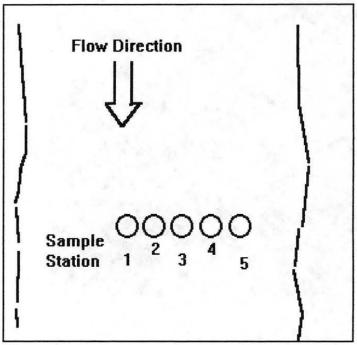

Figure 8

and transfer it into the sampling bags. The armor layer samples are kept in separate bags from the substrate for future differentiation. Figures 10, 11, and 12 show this sampling process in shallow, medium, and deep flow conditions. In the deep flow condition water flows over the top of the barrel, so a filter cloth bag is attached to the barrel to minimize loss of fine material (see Figure 13). This bag is fixed to the barrel by a shock cord, and a small slit (about 5 inches) is cut in the bag, so the sampler can reach his hand into the sampler, take samples off the river bottom, and transfer them into the loose end of the filter bag.. If the bag is filled with substrate material, it is grabbed by the neck and removed from the barrel, while another bag is immediately fixed to the barrel. The samples are removed from the filter bags, and the filters can be flushed to remove any fines that became trapped in them. The samples are transported in army laundry bags to the lab to be tested. (See Figure 14). The advantages of the Modified McNeil sampler include:

    □ There is no limit to the size of material that can be sampled. Unlike the other samplers which are limited by their openings, or the Freeze Core which can not pick up material larger than that in the 64 to 128 mm. range, the Modified McNeil sampler allows any particle found (at least 50% within the sampler) to be sampled.

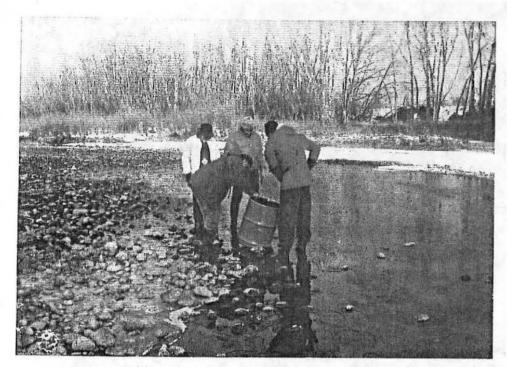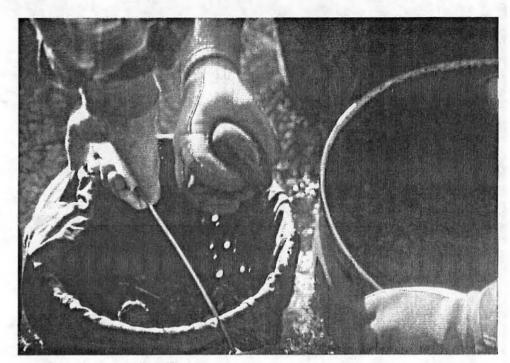   □ Although the sample may is not entirely saved in a stratigraphic sense, the
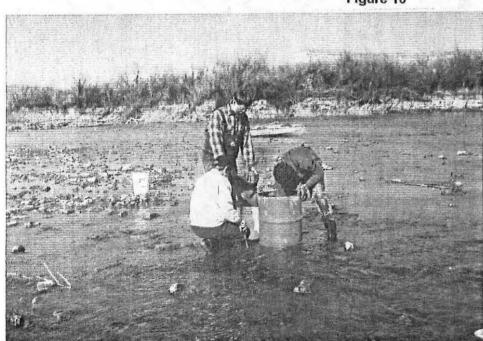
Figure 6

Figure 9

Figure 10

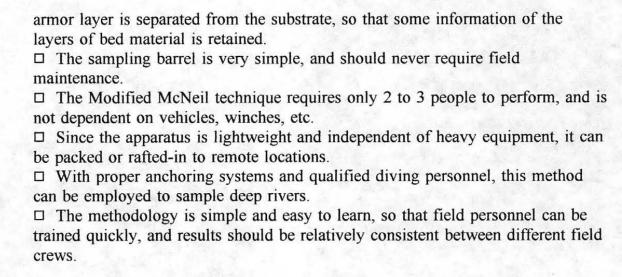Figure 11

Figure 12

Figure 13

Figure 14

armor layer is separated from the substrate, so that some information of the layers of bed material is retained.

☐ The sampling barrel is very simple, and should never require field maintenance.

☐ The Modified McNeil technique requires only 2 to 3 people to perform, and is not dependent on vehicles, winches, etc.

☐ Since the apparatus is lightweight and independent of heavy equipment, it can be packed or rafted-in to remote locations.

☐ With proper anchoring systems and qualified diving personnel, this method can be employed to sample deep rivers.

☐ The methodology is simple and easy to learn, so that field personnel can be trained quickly, and results should be relatively consistent between different field crews.

The main disadvantage of the Modified McNeil sampler is:

■ Some amount of the fines attached to the armor layer may be lost in transferring the armor layer particles to the sample bag.

1.5 Comparison of Chama River Results

To verify the usefulness of the Modified McNeil sampler, and to disclose any weakness in the new methodology, a site which had been previously sampled along the Rio Chama was selected. Samples were taken at two locations within this site (1.2 miles downstream of the El Vado Dam) using the Modified McNeil sampler by Fish and Wildlife, Bureau of Reclamation, and Colorado State University personnel. Just over a year earlier, the Bureau of Land Management sampled the same site.

The flows were similar during both the 1991 and the 1993 sampling sessions. In October 1991, when the area was sampled using the Hubbell and Freeze Core techniques, the flow was about 200 cfs, as it was in January 1993, when the Modified McNeil sampler was employed to sample the same site. The results of both the 1991 Hubbell and Freeze Core samplings, and the 1993 Modified McNeil sampling are presented in Tables 1.1 - 1.12. (Graphs are Figures 15-20). Tables 1.1 - 1.12 show the gradation data for 2 substrates and 2 armor layers (Modified McNeil), 2 Hubbells, and 3 Freeze Cores (for various levels i.e. 0 -10 cm., 10 - 2- cm., 20 - 30 cm.). Graphs or Figures 15 - 20 show the gradation curves for substrate and armor layers (Modified McNeil), Hubbells, and Freeze Cores (0 - 10 cm., and 10 - 20 cm.).

As can be seen in Figure 20, the comparison of results from Hubbell, Freeze Core, and Modified McNeil samplers, the Modified McNeil method can be used to obtain not only larger material than the others, but also fines. Their is an apparent discrepancy observed between the gradations of Modified McNeil armor layers (Tables

Substrate #1	
Sieve Size mm	Percent Passing
152.4	100
101.6	100
76.2	96.88
63.5	94.43
50.8	87.83
38.1	78.79
25	66.86
19	54.01
12.7	46.24
9.5	41.19
4.7	30.25
2.83	25.79
2	22.8
1.41	19.3
1	14.77
0.5	6.47
0.42	5.17
0.354	4.42
0.25	3.01
0.21	2.47
0.125	1.43
0.075	0.79
pan	0.03

Table 1.1

Substrate #2	
Sieve Size mm	Percent Passing
152.4	100
101.6	94.27
76.2	85.44
63.5	78.87
50.8	73.29
38.1	66.85
25	58.94
19	54.48
12.7	48.73
9.5	44.78
4.7	35.49
2.83	29.89
2	26.23
1.41	22.08
1	16.37
0.5	7.43
0.42	6.19
0.354	5.36
0.25	3.57
0.21	2.95
0.125	1.55
0.075	0.84
pan	0.01

Table 1.2

Armor Layer #1	
Sieve Size mm	Percent Passing
152.4	87.02
101.6	82.78
76.2	48.19
63.5	39.5
50.8	21.86
38.1	12.67
25	6.84
19	4.57
12.7	2.85
9.5	2.28
4.7	1.28
2.83	0.78
2	0.59
1.41	0.44
1	0.33
0.5	0.21
0.42	0.19
0.354	0.18
0.25	0.15
0.21	0.14
0.125	0.1
0.075	0.06
pan	0

Table 1.3

Armor Layer #2	
Sieve Size mm	Percent Passing
152.4	100
101.6	100
76.2	93.68
63.5	91.15
50.8	54.8
38.1	32.69
25	11.22
19	7.77
12.7	4.22
9.5	3.14
4.7	1.52
2.83	0.88
2	0.66
1.41	0.48
1	0.34
0.5	0.2
0.42	0.17
0.354	0.15
0.25	0.12
0.21	0.1
0.125	0.06
0.075	0.03
pan	0

Table 1.4

Hubbell #1	
Sieve Size mm	Percent Passing
128	100
64	100
32	78.8
16	66.9
8	57.5
4	48.9
2	42.2
1	32.9
0.5	19.7
0.25	10.3
0.125	4.6
0.063	1.7

Table 1.5

Hubbell #2	
Sieve Size mm	Percent Passing
128	100
64	100
32	89.1
16	75.1
8	65.2
4	57.6
2	51.2
1	38.4
0.5	21.7
0.25	10.9
0.125	4.4
0.063	1.4

Table 1.6

Freeze #9 0-10 cm	
Sieve Size mm	Percent Passing
128	100
64	100
32	73.2
16	50.6
8	38.7
4	32
2	27
1	20.1
0.5	12.6
0.25	7.2
0.125	4
0.063	2

Table 1.7

Freeze #9 10-20 cm	
Sieve Size mm	Percent Passing
128	100
64	100
32	83.9
16	57.7
8	44.2
4	35
2	29.4
1	22.1
0.5	14.7
0.25	8.3
0.125	4.1
0.063	1.8

Table 1.8

Freeze #10 0-10 cm	
Sieve Size mm	Percent Passing
128	100
64	100
32	49.5
16	32.5
8	24.4
4	21.5
2	19.2
1	15.1
0.5	10
0.25	5.9
0.125	3.1
0.063	1.4

Table 1.9

Freeze #10 10-20 cm	
Sieve Size mm	Percent Passing
128	100
64	100
32	87.4
16	57.1
8	43.8
4	33.7
2	28.1
1	20.8
0.5	13.4
0.25	7
0.125	3.3
0.063	1.4

Table 1.10

Freeze #10 20-30 cm	
Sieve Size mm	Percent Passing
128	100
64	100
32	88.3
16	60
8	41.2
4	31.7
2	25.7
1	18.2
0.5	11.6
0.25	6.5
0.125	3.1
0.063	1.3

Table 1.11

Freeze #11 0-10 cm	
Sieve Size mm	Percent Passing
128	100
64	72
32	40.2
16	30.3
8	24.9
4	20.7
2	18.6
1	15.1
0.5	10.5
0.25	7
0.125	4.4
0.063	2.3

Table 1.12

substrate

Figure 15

armor layer

Figure 16

hubbell

Figure 17

freeze core 0-10 cm

Figure 18

freeze core 10 -20 -30 cm

Figure 19

Comparison of Distribution Curves
for Hubbel, Freeze, and Mod. McNeil

Legend:
- ■— freeze core
- ■-- freeze core
- ●— hubbell
- ●— hubbell
- ✳— substrate min
- +— armor layer max
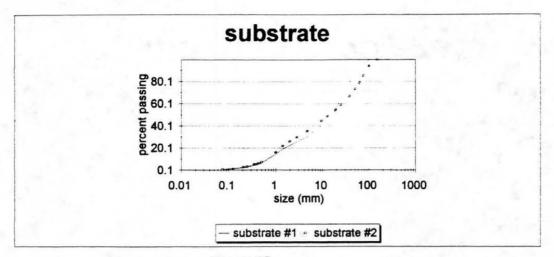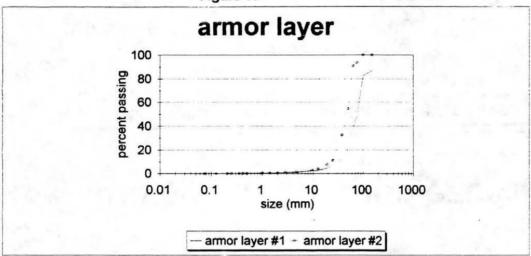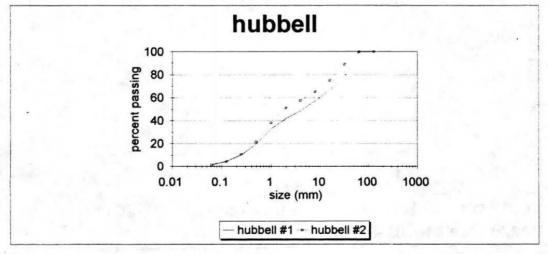
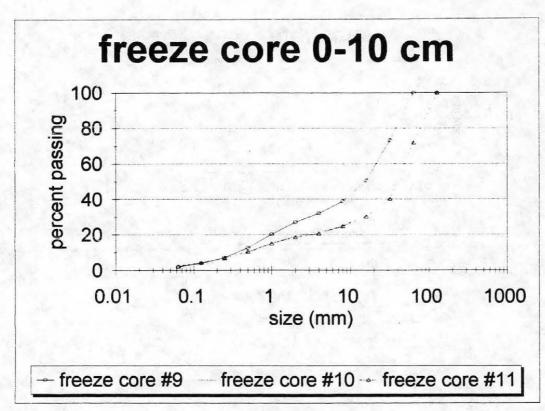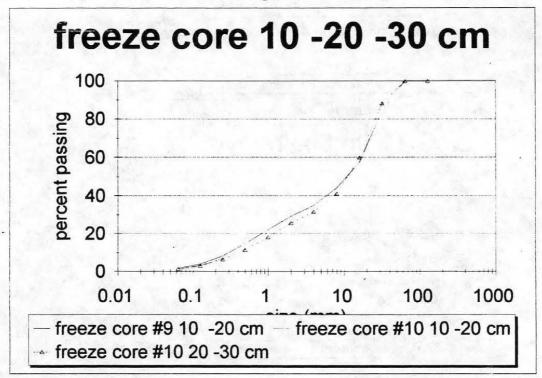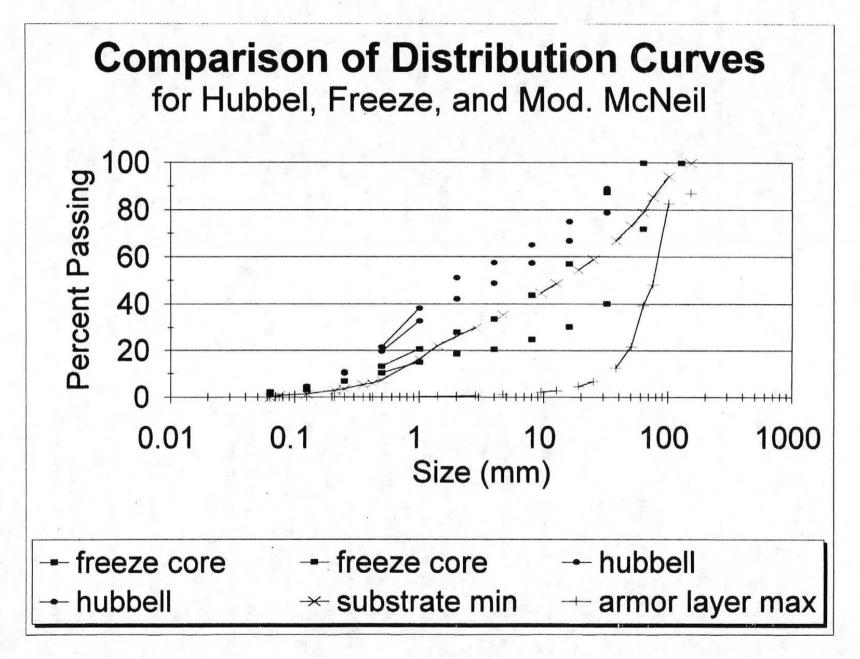**Figure 20**

1.3 and 1.4) and the 0 - 10 cm. Freeze Core results (Tables 1.7, 1.9, and 1.12). These tables and Figure 20 indicate that the Freeze Core method collects more fines in the armor layer. This is probably due to a difference in the definition of armor layers between the two teams performing the sampling. The armor layer, as described in Section 1.4, is only composed of those particles at the surface, not all particles down to a depth of 10 cm. The sample consisting of only the particles exposed to the surface will obviously neglect a great deal of fines down to a depth of 10 cm. If these fines were of concern, they could be obtained by excavating down to 10 cm. and keeping all this material with the armor layer sample.

1.6   Statistical Sample Size

Church, McLean, and Wolcott's methodology in "River Bed Gravels: Sampling and Analysis", 1987, was reviewed and is summarized as follows: It is assumed that the largest class of grains present in the sample will be fewest in number, and therefore should determine the sample size. The percentage of total sample weight that is comprised by the largest stone is evaluated, then from the Sample size (kg) vs. b axis of largest stone (Figure 21) a sample size in kilograms is determined. It should be noted that for a given largest clast size, the sample size (kg) is less for this new method than that which would have been determined using the ISO low precision curve. To see how these curves compare to other commonly used curves, see Figure 22. For an assumed largest clast of 200 mm at 1% of the total sample weight, this would yield an armor layer sample size of about 1100 kg. The armor layer samples taken in 1993 weighed about 240 lbs or 110 kg, or 10% of the suggested sample size. Although the new method by Church, McLean, and Wolcott is more lenient than others used currently, it still demands a relatively large sample. The suggested sample of 1000 kg would be over a ton of armor layer. This amount of bed material would be almost impossible to pack out, would overload most heavy-duty work trucks on the way to the testing facilities, and considering that this is only the armor layer part of the whole sample, might merit a backhoe or other heavy machinery for its excavation.

1.7   Conclusions:

"The characterization of coarse bed material in rivers is difficult because the range of grain sizes is so wide that it is impractical to maintain a single method of measurement." (Church, McLean, Wolcott, 1987). Use of some of the samplers reviewed in this paper would understandably lead to this conclusion. That was one reason for the development of the Modified McNeil sampler. The design of a sampler and sampling technique which could be used widely, under many circumstances, and provide reliable data on fine to larger bed material is indeed an important step toward
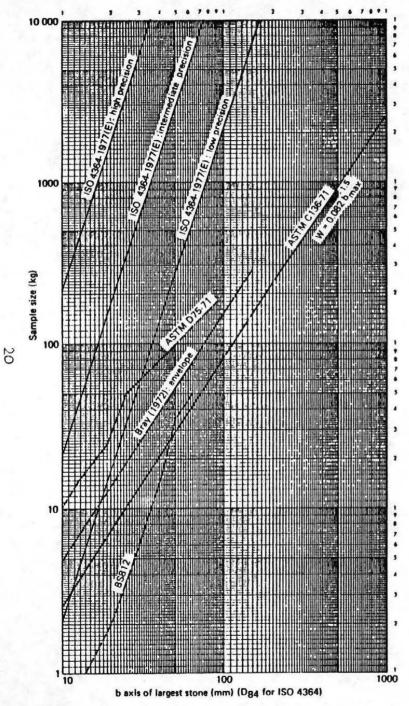
Figure 22 Previously proposed bulk sample standards
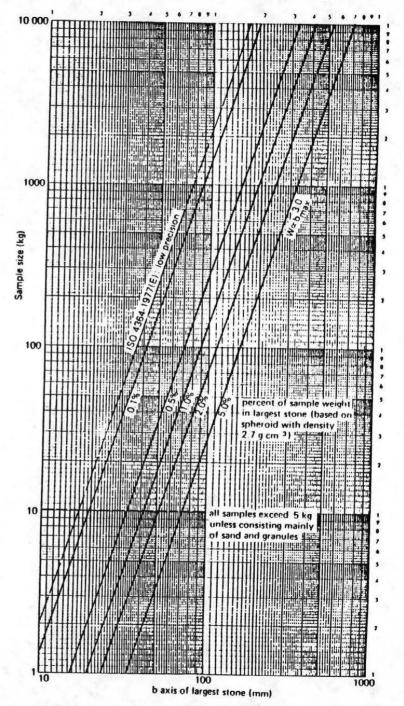

Figure 21 Bulk sample standard for gravels developed in this paper

better understanding of a river's hydraulics, sediment transport, and aquatic habitat.

The Modified McNeil sampler is relatively compact and lightweight, it is not reliant on vehicles, winches, CO_2 tanks, or large operating crews. This sampler is portable, packable, raftable, and can be used to sample larger armor layer material, and also smaller substrate and relatively fine material. This is an important new sampling device because of its simplicity and maintenance free operation, portability, flexibility to sample in low to high flows, and its ability to sample fine and large material.

The Rio Chama results show that the Modified McNeil Sampler can sample the same fine material as a Freeze Core sampler without significant loss of data, while at the same it samples larger material than even the Hubbell sampler can retrieve.

Statistical analysis using the new methodology developed by Church, McLean, and Wolcott, 1987, indicates that for the 1993 Rio Chama armor layer sample to be statistically sound, a 1000 kg sample should have been taken. In this case a sample this large was impractical, and in many cases such a sample is impossible to collect. In the future when more extensive sampling expeditions are taken, larger samples closer to the 1000 kg minimum should be attempted.

1.8   References:

American Society of Civil Engineers. (1977). 'Sedimentation Engineering', New York, NY, 334-337.

Church, M.A., McLean, D.G., and Wolcott, J.F. (1987). 'River Bed Gravels: Sampling and Analysis', Sediment Transport in Gravel-bed Rivers, Thorne, Bathurst, Hey. 43 -87.

Fogg, James L., Hanson, Brian L., Mottl, Henry T., and others. (Dec. 1992). 'Rio Chama Instream Flow Assessment', U.S. Bureau of Land Management, Denver, CO.

Interagency Committee, 'Equipment Used for Sampling Bed Load and Bed Material', Report No. 2, Federal Interdepartmental Committee, Hydraulic Laboratory of the Iowa Institute of Hydraulic Research, Iowa City, Iowa, 1940b.

Swanson, Steve. (1992). 'Results from Rio Chama Instream Flow Assessment', U.S.B.L.M., Denver, CO.

Thorne, C.R., Bathurst, J.C., and Hey, R.D. (1987). 'Sediment Transport in Gravel-bed Rivers', New York, John Wiley & Sons Ltd. 43-87.

COMPARISON OF SEDIMENT TRANSPORT CALCULATIONS
GIVEN MULTIPLE SEDIMENT SAMPLES AT A SINGLE CROSS SECTION

BY

Dan Gessler[1]

ABSTRACT

When multiple sediment samples are collected in a channel, inevitably there is a degree of variability between the resulting grain size distributions. When the variability is large, a problem arises in selecting the appropriate grain size distribution for sediment transport calculations. This paper presents the results of a case study on a single cross section of a creek in central Mississippi. Yang's sediment transport equation was used to compute sediment transport by size fraction. Sediment rating curves were computed for the section using various appropriate grain size distributions.

INTRODUCTION

Colorado State University is currently working in conjunction with the U.S. Army Corps of Engineers on the Demonstration Erosion Control (DEC) project in central and northern Mississippi. The objective of the project is to help find a suitable means for stabilizing channels that are actively incising. Achieving this objective requires that topographical surveys be conducted and sediment samples collected in 20 study reaches on an annual basis. Preliminary results of the 1992 sediment sampling program indicate that in some study reaches, there is a high degree of variability between grain size distributions obtained from samples collected at different locations in the same cross section. Variations of D_{50} were noted to exceed a factor of three while variations in D_{85} exceeded a factor of 15. This presents a problem when deciding which grain size distribution to use for sediment transport calculations. This paper presents the results of a detailed analysis of this problem at a single cross section on Harland Creek.

[1]   Graduate Research Assistant, Department of Civil Engineering, Colorado State University, Fort Collins, Colorado, 80523

DESCRIPTION OF DATA FOR ANALYSIS

Data collected in the 4000 foot Harland Creek study reach included a thalweg and cross section survey (conducted in May 1992), and over thirty sediment samples. At any given cross section, a maximum of four surface sediment samples was collected. The location of each of the samples relative to the left toe of slope was recorded. One of the nine cross sections surveyed was selected for this study. The location of the section relative to the study reach is shown in figure 1. From carefully looking at figure 1, it can be seen that the cross section is located in a bend to the right. Each x in figure 1 represents a surveyed topographical point.
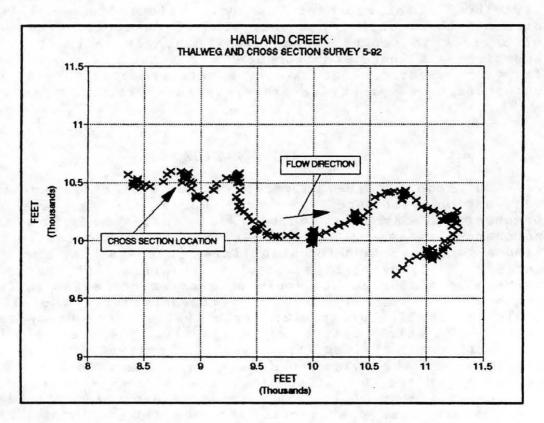

Figure 1
Plan view of study reach survey

Thalweg survey points were used to generate a profile of the channel bottom. A linear regression through the points was used to determine the average bed slope in the reach. The bed profile and regression line are shown on the following page in figure 2.

Gessler
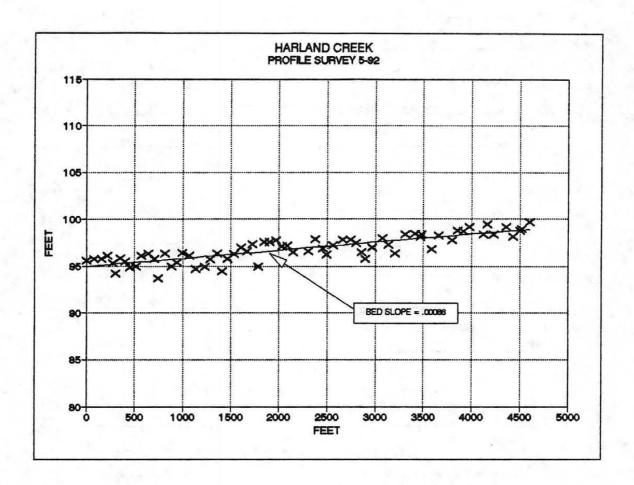
Figure 2
Channel profile

Figure 3 shows the cross section (looking downstream) with the location of the sediment samples collected. Also shown in figure 3 is the segment delineation used for sediment transport calculations. In each segment, a single sediment sample was collected.

Figure 4 shows the grain size distribution for each of the samples collected. It is worth noting that the finest grain size distribution was located in segment 4 on the right bank which is on the inside of the bend. The coarsest material was found in segment 2 near the channel thalweg.

Figure 3
Channel cross section

Figure 4
Grain size distributions of samples collected.

Gessler

SEDIMENT TRANSPORT CALCULATIONS

Five different scenarios were considered for comparison of the sediment transport rates. In each case, Yang's sediment transport equation was used. Yang's equation requires that the se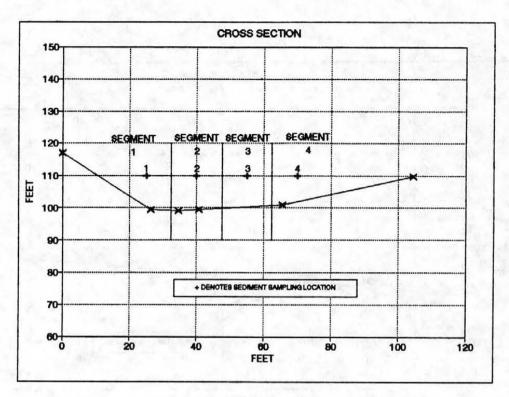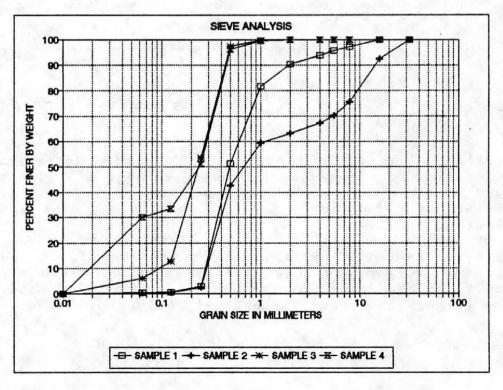diment transport be computed by size fraction. Furthermore, the equation is actually two relationships; one being used for sand particles one millimeter in diameter and smaller and a second relationship being for gravels larger than one millimeter in diameter. In each case, the sediment transport is calculated for flow depths of 2, 4, 6, and 8 feet. What follows is a brief description of each procedure:

Transport by Channel Segmentation

The cross section is divided into 4 segments as shown in figure 3. In each segment i, Manning's n is determined using the Strickler formula shown below.

$$n_i = 0.039 * k_s^{1/6}$$

$n_i = Mannings \ n$
$k_s = D_{95} \ (feet)$

If it is assumed that Manning's equation applies in each segment and that the velocity in each segment is the same as the average velocity in the channel then the following relationship holds true for each segment i.

$$V = \frac{1}{n_i} R_i^{2/3} S^{1/2}$$

From this equation, it follows that a composite Manning's n can be computed for the cross section. The composite Manning's n can then be used to compute the discharge and velocity at a given water surface elevation for the entire section as well as for each segment. (If the sediment transport rate is computed at given water surface elevations rather than at fixed discharges, a direct solution can readily be found for the problem.) It is now possible to compute the sediment transport in each segment using the grain size distribution determined for that segment. The sum of the transport in all of the segments gives the total transport in the section.

Gessler

Transport by Average Distribution

An alternative to computing the sediment transport in each segment and then adding them, is to average all of the sediment samples collected at the section. The average distribution is then used to compute an average Manning's n from the Strickler formula. Using Manning's equation the velocity and discharge can be found at the same four water surface elevations discussed earlier. The sediment transport rate can now be computed for the average grain size distribution for the entire cross section.

Transport by Maximum and Minimum Distribution

By computing the sediment transport rates for the entire cross section using only the finest or coarsest sediment sample (2 and 4 respectively) an 'envelope' can be found within which the actual sediment transport rate should lie. It is worth noting that if only one sediment sample had been collected rather than four, there would be a fifty percent chance that it would be one of the two extreme samples.

Transport by Average D_{50}

Since the computation of sediment transport by size fraction is a fairly time consuming process, one might be tempted to make only one calculation using D_{50}. Therefore, the sediment transport was calculated assuming a uniform grain size distribution of the diameter of D_{50}.

Yang's Sediment Transport Equation

Yang's sediment transport equation is comprised of two relationships; one gives the sediment transport rate for sand while the other gives the sediment transport for gravels. Though the equations can be looked up in several books, it is included on the following page for completeness.

For Sand:

$$LogC_t = 5.435 - 0.286*Log\left(\frac{\omega d_s}{\nu}\right) - 0.457*Log\left(\frac{u_*}{\omega}\right)$$

$$+\left(1.799 - 0.409*Log\left(\frac{\omega d_s}{\nu}\right) - 0.314*Log\left(\frac{u_*}{\omega}\right)\right)*Log\left(\frac{VS}{\omega} - \frac{V_c S}{\omega}\right)$$

where

C_t = sediment concentration (ppm by weight)
ω = fall velocity (m/sec)
d_s = particle size (m)
ν = kinematic viscosity (m²/s)
u_* = shear velocity = $\sqrt{\tau/\rho}$
τ = shear stress (N/m²) = γRS
γ = specific weight of water (N/m³)
R = hydraulic radius (m)
S = energy slope (m/m)
ρ = density of water (kg/m³)

$$V_c/\omega = \frac{2.5}{Log(u_* d_s/\nu) - 0.06} + 0.66$$

for

$$2 \leq \frac{u_* d_s}{\nu} \leq 70$$

For Gravel:

$$LogC_t = 6.681 - 0.633*Log\left(\frac{\omega d_s}{\nu}\right) - 4.816*Log\left(\frac{u_*}{\omega}\right)$$

$$+\left(2.784 - 0.305*Log\left(\frac{\omega d_s}{\nu}\right) - 0.282*Log\left(\frac{u_*}{\omega}\right)\right)*Log\left(\frac{VS}{\omega} - \frac{V_c S}{\omega}\right)$$

Gessler

RESULTS

Results of the calculations are presented in figure 5. The horizontal axis shows discharge in cubic meters per second while the vertical axis gives the sediment transport in metric tons per day.
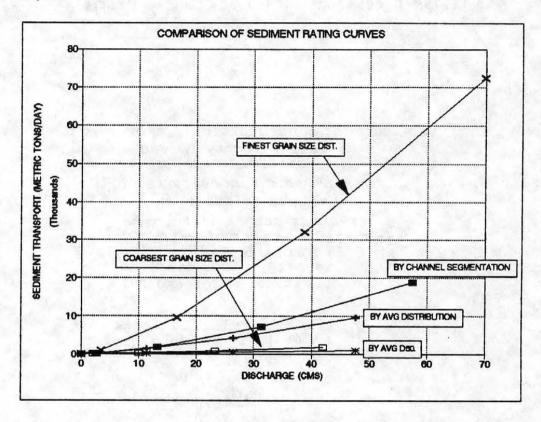
Figure 5
Comparison of sediment rating curves.

In order to evaluate the results of using the method of channel segmentation, two additional plots are necessary. Figure 6 shows the cumulative amount of sediment transported in each segment. The horizontal axis gives the discharge in cms and the vertical axis gives the sediment transport in metric tons per day. Figure 6 demonstrates that at flows exceeding 20 cms segment 4 carries over 50 percent of the total sediment transport. This is due to the relatively fine sediment found in segment 4. To further demonstrate this point, figure 7 shows the cumulative amount of sediment transported in four particle size groups. Over 75 percent of the particles transported have a diameter of 0.063 to 0.125 mm. Approximately 40 percent of the material in segment 4 falls into this category. Particles over 2 mm in diameter comprise less than one percent of the material transported.

Gessler

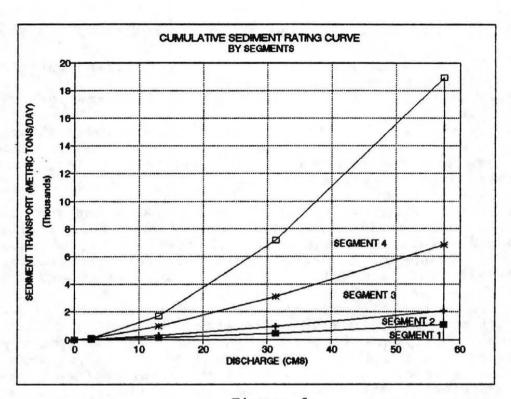**Figure 6**
Cumulative sediment rating curves by cross section segments.
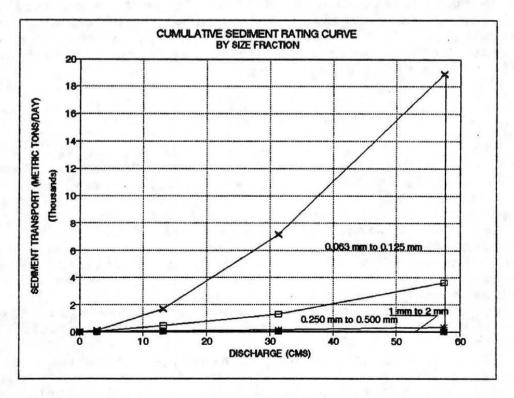

Figure 7
Cumulative sediment rating curves by size fraction.

Gessler

DISCUSSION OF RESULTS

The difference between the sediment rating curve computed using the coarsest sample and that computed using the finest sample is very large. At a discharge of 20 cms they differ by approximately one order of magnitude and at a discharge of 40 cms, they differ by over 1.5 orders of magnitude. This clearly demonstrates the need for a well designed sediment sampling program and the importance of collecting a large number of samples in a mixed bed channel.

The sediment rating curve computed when assuming a uniform grain size of D_{50} falls slightly below that found when using the coarsest grain size distribution. Clearly this approximation under predicts the sediment transport rate. At a discharge of 40 cms it appears to under predict the sediment transport by a full order of magnitude. It is this authors opinion that this approximation should not be used.

In comparing the method of channel segmentation with that of using a single average grain size distribution it can be seen that at low flows (less than 25 cms) the two are remarkably similar. As the discharge increases beyond 25 cms segment four begins to transport a significant amount of sediment (see figure 6). Segment four contains material that is of a very fine nature with a D_{50} of only 0.25 mm that is readily transported. Therefore, once segment four becomes inundated, the sediment transport increases very rapidly. It is this authors opinion that using an average distribution provides a suitable approximation for estimating sediment transport rates. It is unclear whether any real improvement in the approximation is derived from using channel segmentation.

CONCLUSIONS AND DISCUSSION

This paper has clearly demonstrated that great care must be taken when collecting sediment samples. Figure 5, 'Comparison of Sediment Rating Curves', showed that the 'envelope' in which the actual sediment transport rate should be found is very large. It is therefore important to insure that samples collected are representative of material found in the channel. Unfortunately, there is no set procedure that can be applied to every channel that will guarantee that representative samples are collected. The collection of sediment samples will always require a certain degree of judgement by the investigator. By collecting a large number of samples and averaging them, the impact of an 'outlier' sample on transport calculations is minimized.

In comparing the method of channel segmentation and the use of average grain size distribution, the two methods appear to yield fairly similar results. This is particularly apparent when comparing the difference between the two methods to the

size of the transport envelope. For the case investigated, there is no reason to believe that the method of channel segmentation conclusively yields a more accurate result. During the collection of sediment samples for this project, it was not anticipated that sediment transport might be computed by channel segmentation. This resulted in a potential weaknesses in the method. Only one sediment sample was collected in each segment. If the sample collected was an outlier for that segment, the subsequent transport calculations in the segment would be erroneous. If the channel is segmented during the collection of the field data, multiple samples can be collected in each segment. This would serve to increase the reliability of the grain size distribution in the segments.

There are many other important parameters in sediment transport calculations, other than grain size distribution, that also have a degree of uncertainty associated with them. For example, one might consider the energy slope of the water. The uncertainty in transport calculations due to the inability to accurately determine this parameter may far out weigh the improved accuracy of using channel segmentation. This factor was beyond the scope of this paper, however, it should be investigated in future research. Additional research should also include field measurements of actual sediment transport rates in the channel segments. This is necessary to verify that physical reality is related to the conceptual model. The author believes that the two may differ on the sloping banks of the channel. This stems form the fact that much of our knowledge of sediment transport is based on flume studies conducted in rectangular flumes. Relatively little is known about sediment transport rates on sloping banks.

EVALUATING CONTRACTION SCOUR AT BRIDGES USING SEDIMENT TRANSPORT RELATIONSHIPS

L. A. Arneson

Abstract

Computing contraction scour through bridge openings using conventional techniques that assume fixed bed conditions may overestimate the amount of contraction scour that results. The currently recommended procedures for estimating contraction scour rely on methods that do not account for decreasing hydro-dynamic forces through the bridge opening as a result of increased cross-sectional area. This paper will examine contraction scour through bridge openings and through an example, demonstrate that the ultimate depth of scour can be overestimated if the forces that cause contraction scour are not adequately considered.

Introduction

In this paper contraction scour will be estimated for a hypothetically constructed bridge using conventional modeling and analysis techniques. Contraction scour will then be evaluated for the same bridge using sediment transport relationships in a computer model capable of simulating hydraulic conditions through a bridge opening simultaneously with sediment transport.

Contraction Scour

Contraction scour is the result of flow velocities through a bridge opening higher than what would occur without the bridge in place. The increased velocity caused by constricting the flow, transports material out of the opening until the hydro-dynamic forces are no longer sufficient to transport sediment. If a bridge opening, and the reach of river immediately upstream and down, can be thought of as a control volume, contraction scour can be broken into two classifications. Live-bed sediment transport occurs where there is a sediment flux across the upstream boundary of the control volume and clear-water sediment transport occurs when there is no sediment flux across the upstream boundary.

The Federal Highway Administration's (FHWA's) Hydraulic Engineering Circular (HEC) No. 18, Evaluating Scour at Bridges[1] and Hydraulic Engineering Circular No. 20, Stream Stability at Highway Structures[2] present information and equations that can be used to evaluate scour at bridges that consists of long term aggradation or degradation, contraction scour, and local scour at piers and abutments. Much consideration has been given to the

equations that best compute the various components of local scour, such as those that occur at piers, abutments, and through contracted sections caused by bridges. The currently recommended procedures for estimating live-bed and clear-water contraction scour with fixed bed bridge hydraulics are presented by Laursen[3]. These methods are discussed in the following sections.

<u>Live-Bed Contraction Scour</u>

The live-bed contraction scour equation presented by Laursen and recommended in HEC-18 is:

$$\frac{y_2}{y_1} = \left[\frac{Q_{mc2}}{Q_{mc1}}\right]^{\frac{6}{7}} \left[\frac{W_{C1}}{W_{C2}}\right]^{k_1} \left[\frac{n_2}{n_1}\right]^{k_2} \ldots (1)$$

where:

$y_1 =$ average depth in the main channel at the "approach" cross-section, ft.,
$y_2 =$ average depth in the contracted section, ft.,
$Q_{mc1} =$ flow in the approach main channel that is transporting sediment, cfs,
$Q_{mc2} =$ flow in the contracted main channel which is often Q_{total}, but not always, cfs,
$W_{c1} =$ average bottom width of the main channel at the "approach" cross-section, ft.,
$W_{c2} =$ average bottom width of the contracted section, ft.,
$n_2 =$ Manning's n for the contracted section,
$n_1 =$ Manning's n for the main channel, and
K_1 & $K_2 =$ exponents described in HEC-18.

The estimated contraction scour, y_s, can then be estimated by subtracting y_1 from y_2, ie. $y_s = y_2 - y_1$, ft.

In a flood, flow is typically in the overbank during the event for which the contraction scour is to be estimated. The above relationship assumes that the material being transported is in the main channel, therefore, the flow parameters needed for the computation are for the main channel only. The problem then becomes separating the flow in the main portion of the channel from the flow in the overbank area. This task is readily accomplished using FHWA's Bridge Backwater Analysis Computer Program, WSPRO[4,5] to develop hydraulic parameters at the "approach" and "bridge" cross-sections. Figure 1 illustrates the parameters necessary for the contraction scour computations.
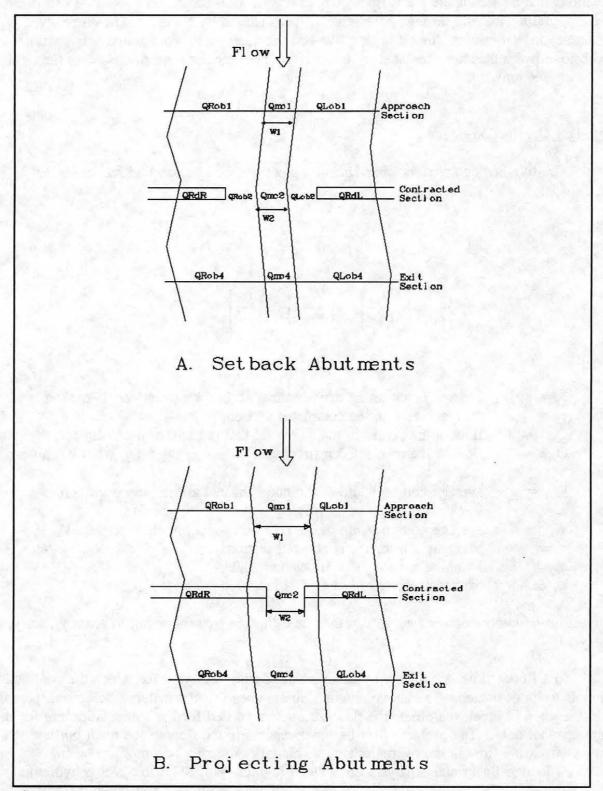
A. Setback Abutments

B. Projecting Abutments

Figure 1 - Contraction Scour Variable Definition

Contraction scour can be estimated for all of the typical cases of live-bed scour illustrated in HEC-18 and Figure 1 using the above equation and WSPRO to determine the hydraulic variables in each portion of the floodway. For the cases where the abutments encroach into the main channel or are at the edge of the main channel the procedure used to compute the hydraulic parameters is straight forward. However, when the abutments are set back into the overbank and the entire bridge opening does not experience live-bed scour, the value of Q_{mc2} and W_{mc2} should be determined for the portion of the channel where the live-bed scour occurs. The contraction scour for the overbank portion of the contracted section when there is clear-water scour can be estimated using the following relationships.

Clear-Water Contraction Scour

The two HEC-18 recommended equations for determining clear-water contraction scour when part of the bridge opening experiences clear water-scour are:

$$Y_{ob2} = [Q_{ob2}^2/(120\ D_{50}^{2/3}\ W_{setback}^2)]^{3/7} \ \cdot\ \cdot\ \cdot\ (2)$$

and

$$Y_{sob} = Y_{ob2} - Y_{ob1} \ \cdot\ \cdot\ \cdot\ (3)$$

where:

y_{ob1} =   average depth in the left or right overbank at the uncontracted "approach" cross-section, ft.,

y_{ob2} =   flow depth in the left or right overbank in the contracted section, ft.,

y_{sob} =   depth of scour in the left or right overbank of the contracted section, ft.,

Q_{ob2} =   discharge in the left or right overbank portion of the contracted section, cfs,

D_{50} =   sediment size in the overbank portion of the contracted section, ft., and

$W_{setback}$ =   distance the abutment is set back from the main channel, ft.

The depth of scour, y_{sob}, in the left or right overbank of the contracted section is computed using Equation 3 by subtracting y_{ob1} from y_{ob2}.

The above equation applies to the case where the abutment is set back into the overbank and there is no live-bed scour in the overbank portion of the contracted section. Often it is difficult to determine whether or not the scour is a result of live-bed or clear-water sediment transport. Methods that use critical shear stress or critical velocity can be used to determine whether the scour process is live-bed or clear-water.

Sediment Transport Modeling

The sediment transport modeling has been accomplished using the BRI-STARS (**BRI**dge **S**tream **T**ube model for **A**lluvial **R**iver **S**imulation) computer model[6]. This model has the capability to:

- Compute hydraulic parameters for open channels with fixed as well as alluvial boundaries,
- Compute, through the use of energy and momentum concepts, water surface profiles for subcritical, supercritical, and combinations of both flows without interruption,
- Compute and simulate, through the use of "streamtubes", hydraulic and sediment conditions in longitudinal and lateral directions,
- Compute and simulate, using concepts of minimum rate of energy dissipation, the change of alluvial channel profile and geometry regardless of whether the channel width is variable or fixed.

The model is designed such that it can be used in varying levels of complexity. For example, if analysis of fixed bed bridge hydraulics is desired, the model can be operated with only the records necessary for fixed bed analysis. If sediment transport is desired, information necessary for the sediment transport computations can be added. If changes in channel geometry are desired using concepts of minimum rate of energy dissipation, additional records are added which specify the analysis parameters.

The BRISTARS model routes sediment through "streamtubes" which are visualized as portions of the channel bounded by imaginary lines to which, at each instant, velocity vectors are tangent. Thus in "streamtubes" with smaller depths and velocities sediment transport will not be as great as in those tubes with higher depths and velocities. This makes it possible to model aggradation and degradation simultaneously in the same cross-section. For each "streamtube" the sediment routing computations are performed by satisfying the sediment continuity relationship which is given as:

$$\frac{\partial Q_s}{\partial x} + n\frac{\partial A_d}{\partial t} + \frac{\partial A_s}{\partial t} - q_s = 0 \ldots (4)$$

where:

$n =$ the volume of sediment in a unit bed layer volume,
$A_d =$ the volume of sediment deposition per unit length of channel,
$A_s =$ the volume of sediment in suspension at the cross-section per unit length,
$Q_s =$ the volumetric sediment discharge, and
$q_s =$ the lateral sediment inflow.

The computer program has the capability to model sediment transport using several different transport relationships. Although other sediment transport equations were examined, results

using Yang's sand and gravel equations[7,8] will be presented in this paper.

Analysis Procedure

The procedure followed to analyze the difference in contraction scour estimates using Laursen's method and the procedure that applies sediment transport relationships through a bridge opening will be accomplished in four steps. First, develop a reach of river and a hypothetical bridge at which contraction scour can be estimated. Second, use WSPRO to develop hydraulic parameters necessary to estimate contraction scour using Laursen's methods. Third, model the contraction scour using sediment transport relationships and the BRISTARS computer model. Fourth, discuss the results and determine if any conclusions are warranted. The reach of river and hypothetical bridge are described in the next section.

Statement of Problem

A 650-foot-long Type 3 (spill-through abutments and sloping embankments) bridge has been developed for which the contraction scour is to be evaluated. The bridge is constructed over a channel which has an estimated design flow of 30,000 cfs. The right abutment is fixed at the right bank of the main channel and the left abutment extends into the overbank area. The elevation of the bridge deck is 22 feet and the girder depth is 4 feet. Six round nose piers that are 5 feet thick and 40 feet long will be placed in the channel. Four piers are in the main channel and two are in the overbank area. The abutments are on 2:1 slopes. The abutments and piers are designed to be aligned with the flow. Long term aggradation and degradation have been considered and are assumed to be negligible. The D_{50} of the bed material is assumed to range from 1 mm to 10 mm in six different estimates of contraction scour. The estimates of contraction scour are completed using Laursen's methods and the BRISTARS computer model.

Laursen's Method

A data deck to analyze the bridge configuration presented in the statement of problem has been developed to run with the WSPRO computer program that produces output from which the variables necessary to compute contraction scour can be determined. Since the bridge opening contains both the main channel and a portion of the overbank, it is assumed that contraction scour will result from both live-bed and clear-water contraction scour. Using equations 1 through 3 contraction scour has been computed for each of the sediment sizes. The contraction scour in the main channel of the bridge opening has been computed to be 6.8 feet for each sediment sizes. The depth of scour in the overbank portion of the bridge opening ranges from 2.0 feet for a sediment size of 1 mm. to no contraction scour for a sediment size of 4 mm.. The results of the analysis are shown in table 1.

Sediment Transport Relationships

Input decks to analyze the flow situation for each of the sediment sizes have been developed that compute contraction scour through the bridge opening. Scour has been estimated at four cross-sections. The approach cross-section is located at station 2050 (one bridge length upstream of the bridge), the second cross-section is located at station 1450 (the upstream face of the bridge), the third cross-section is located at station 1400 (the downstream face of the bridge), and the exit cross-section at station 750 (one bridge length downstream of the bridge). The amount of contraction scour for each of the sediment sizes has been computed at each of the cross-sections. In general, there is aggradation at the upstream and downstream cross-sections and scour at both cross-sections in the bridge opening. Table 2 summarizes the depth of scour at each cross-section for each sediment size. The scour depths for the 1 and 2 mm. sediment sizes do not behave as expected because of instabilities in the simulation. Either the time step is too large or the distance between cross-sections too long. The 4 mm. and larger sizes show in general about 0.30 foot of deposition at the approach cross-section, 4.30 feet of scour at the upstream face of the bridge, 3.30 feet of scour at downstream face of the bridge, and 1.40 feet of deposition at the exit cross-section. Scour in the overbank portion of the bridge opening is about 0.80 foot.

Results

From the results of the analysis, the following comments are offered:

- The depth of scour computed with sediment transport relationships is about 40 percent less than when computed with Laursen's live-bed contraction scour equation.

- Scour depth in the overbank area averages about 0.80 foot which is greater than the amount of scour computed with Laursen's clear-water scour relationship for sediment sizes larger than 2 mm..

- The amount of contraction scour is not dependent on the size of the bed material. This results from the fact that shear stress through the bridge opening is large compared to the critical shear stress for each of the particle sizes. Also, Laursen's equation for live-bed contraction scour is not dependent on sediment size. Figure 1 shows scour depth as a function of time for each of the sediment sizes modeled. Critical shear stress is computed for each sediment size and is presented in table 1. Figure 3 shows plots of energy gradient and shear stress vs. distance.

- The depth of scour predicted with Laursen's equation for clear-water scour is a function of sediment size. For this example, Laursen's method predicts zero contraction scour for sediment sizes larger than 4 mm.. Contraction scour predicted with sediment transport relationships average about 0.80 foot in the overbank portions of the bridge opening. Figure 4 shows the amount of contraction scour or deposition

at each of the cross-sections.

- Backwater is significantly reduced as the cross-sections at the bridge opening are enlarged because of the contraction scour process. Figure 2 shows the water surface and bed profile for several time intervals. The 4 mm. sediment size is considered representative.

- The contraction scour estimates were computed using Yang's sand and gravel relationships for sediment transport. Other sediment transport relationships produce similar results.

Summary and Conclusions

Estimating contraction scour using conventional techniques to determine the hydraulic variables and Laursen's method may tend to overestimate the amount of contraction scour that may actually occur. This could lead to bridge foundations too conservatively designed. Although models to analyze bridge hydraulics in conjunction with sediment transport are more costly to apply, the resulting savings in foundation cost could justify the additional expense. Additionally, one of the design criteria usually applied when specifying the length of a new or replacement bridge is the amount of backwater the bridge creates during the design flood. It is demonstrated in this analysis that the amount of backwater decreases as contraction scour develops. Recognizing this fact would allow bridges to be designed more in accordance with reality.

1. Richardson, E.V., Harrison, L.J., and Davis, S.R., Evaluating Scour at Bridges, FHWA-IP-90-017, February 1991.

2. Lagasse, P.F., Schall,J.D., Johnson, F., Richardson E.V., Richardson, J.R., and Chang, F., Stream Stability and Scour at Highway Structures, FHWA-IP-90-014, February 1991.

3. Laursen, E. M., "Scour At Bridge Crossings," Journal Hydraulics Division, ASCE Vol. 89, No. HY3, May 1960, pp. 93-118.

4. Shearman, J. O., User's Manual for WSPRO -- A Computer Model for Water Surface Profile Computations, FHWA-IP-89-027, September, 1990.

5. Arneson, L. A., Shearman, J.O., Jones, J.S., Evaluating Scour at Bridges Using WSPRO, 1992 Transportation Research Board Meeting, January 1992.

6. Molinas, A., "User's Manual For BRI-STARS", National Cooperative Highway Research Program - Project No. HR 15-11, June, 1992.

7. Yang, C.T., "Incipient Motion and Sediment Transport," Journal of the Hydraulics Division, ASCE, Vol. 99, No. HY10, October 1973.

8. Yang, C.T., "Unit Stream Power Equation for Gravel," ASCE Journal of the Hydraulics Division, Vol. 110, No. HY12, December 1984.

Table 1. - Contraction Scour - Laursen's Method

Contraction Scour Calculations - Main Channel, Case 1a
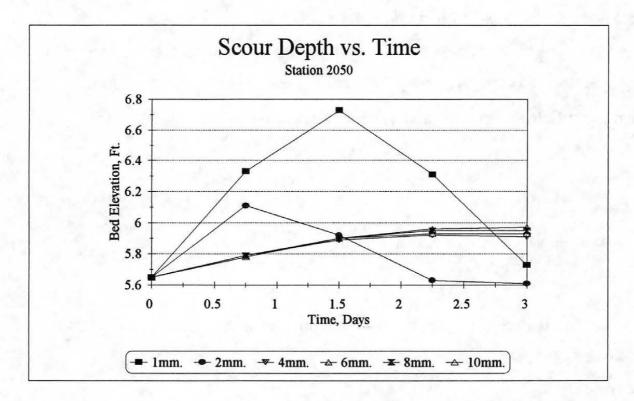
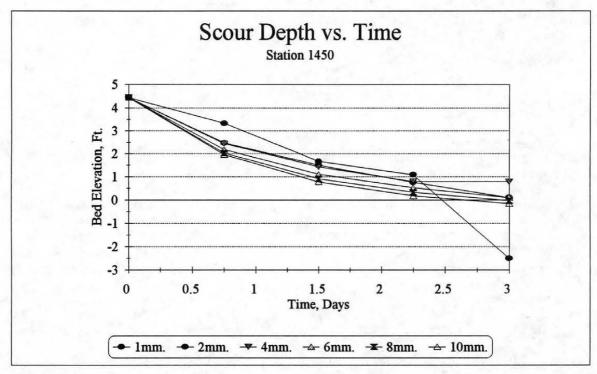| Q	Y2	Y1	Qmc2	Qmc1	Wc1	Wc2	K1	N2	N1	K2	Ys
30000	15.5	8.7	27176.4	14438.8	400	380	0.64	0.032	0.032	0.21	6.8

Contraction Scour Calculations - Overbank, Clear Water Scour
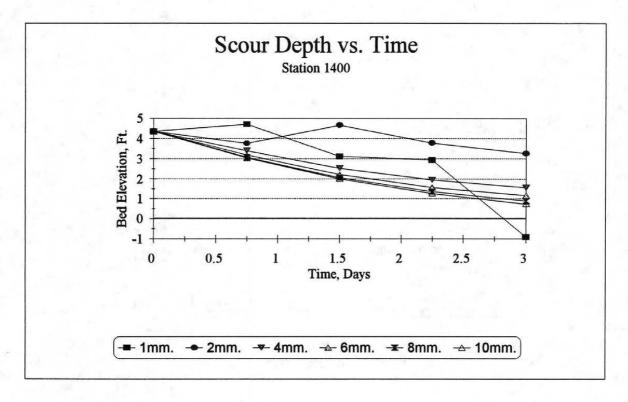
D50 mm.	Q	Y2	Y1	Qob2	D50 ft.	Wset	Ys	Critical Shear Stress, lbs./ft.^2
1	30000	6.1	4.1	2823.6	0.0033	211	2.0	0.01588
2	30000	5.0	4.1	2823.6	0.0066	211	0.9	0.03175
4	30000	4.1	4.1	2823.6	0.0131	211	0.0	0.06350
6	30000	4.1	4.1	2823.6	0.0197	211	0.0	0.09526
8	30000	4.1	4.1	2823.6	0.0262	211	0.0	0.12701
10	30000	4.1	4.1	2823.6	0.0328	211	0.0	0.15876
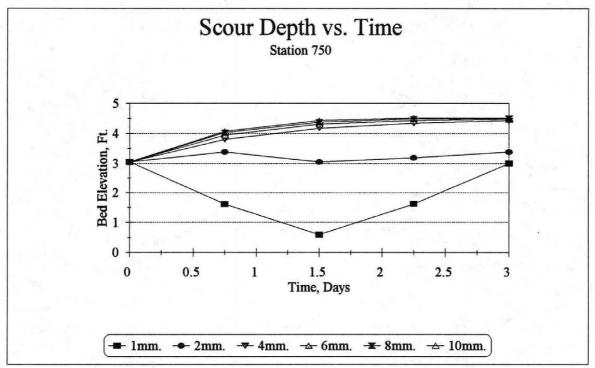
Table 2. - Contraction Scour - Sediment Transport Relationships
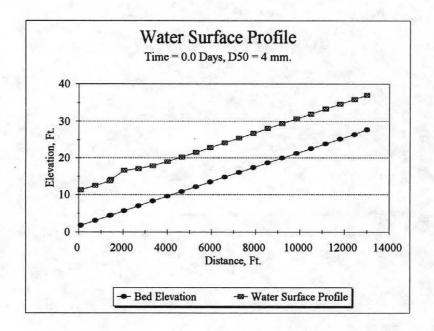
Initial Bed Elevations   5.65   4.45   4.35   3.05
Time Step - 0.05 Days   Simulation Duration - 3.0 Days   Number of Stream Tubes = 3

Sediment Size = 1mm.

Time	Station	2050	1450	1400	750
		Scour Depth			
0.00		0.00	0.00	0.00	0.00
0.75		0.68	-1.12	0.36	-1.44
1.50		1.08	-2.78	-1.23	-2.45
2.25		0.66	-3.36	-1.41	-1.43
3.00		0.08	-6.95	-5.26	-0.05

Sediment Size = 2mm.

Time	Station	2050	1450	1400	750
		Scour Depth			
0.00		0.00	0.00	0.00	0.00
0.75		0.46	-1.98	-0.59	0.33
1.50		0.27	-2.95	0.32	0.00
2.25		-0.02	-3.69	-0.56	0.14
3.00		-0.04	-4.35	-1.08	0.34

Sediment Size = 4mm.

Time	Station	2050	1450	1400	750
		Scour Depth			
0.00		0.00	0.00	0.00	0.00
0.75		0.14	-2.00	-0.95	0.76
1.50		0.24	-3.03	-1.81	1.13
2.25		0.27	-3.65	-2.39	1.30
3.00		0.26	-3.66	-2.77	1.38

Sediment Size = 6mm.

Time	Station	2050	1450	1400	750
		Scour Depth			
0.00		0.00	0.00	0.00	0.00
0.75		0.14	-2.27	-1.16	0.90
1.50		0.25	-3.34	-2.13	1.26
2.25		0.28	-3.93	-2.77	1.38
3.00		0.28	-4.35	-3.19	1.42

Sediment Size = 8mm.

Time	Station	2050	1450	1400	750
		Scour Depth			
0.00		0.00	0.00	0.00	0.00
0.75		0.14	-2.42	-1.27	0.98
1.50		0.25	-3.54	-2.28	1.33
2.25		0.30	-4.12	-2.98	1.44
3.00		0.30	-4.48	-3.46	1.45

Sediment Size = 10 mm.

Time	Station	2050	1450	1400	750
		Scour Depth			
0.00		0.00	0.00	0.00	0.00
0.75		0.13	-2.49	-1.31	1.03
1.50		0.25	-3.67	-2.35	1.38
2.25		0.31	-4.27	-3.08	1.47
3.00		0.32	-4.61	-3.61	1.47

L.A. Arneson

Figure 1. - Scour Depth vs. Time

Figure 1. - Scour Depth vs. Time (cont.)   12

Scour Depth vs. Time
Station 1400

Legend: 1mm. ● 2mm. ▼ 4mm. △ 6mm. ✱ 8mm. △ 10mm.

Scour Depth vs. Time
Station 750

Legend: 1mm. ● 2mm. ▼ 4mm. △ 6mm. ✱ 8mm. △ 10mm.

44

Figure 2. - Water Surface Profiles 13

Water Surface Profile
Time = 0.0 Days, D50 = 4 mm.

Water Surface Profile
Time = 0.75 Days, D50 = 4 mm.

Water Surface Profile
Time = 1.50 Days, D50 = 4 mm.

Figure 2. - Water Surface Profiles (cont.)   14

Water Surface Profile
Time = 2.25 Days, D50 = 4 mm.

Water Surface Profile
Time = 3.0 Days, D50 = 4 mm.

46

Figure 3. - Energy Gradient and Shear Stress vs. Distance   15

Energy Gradient
D50 = 4 mm.

— 0.00 Days —⊗— 0.75 Days —▼— 1.50 Days —△— 2.25 Days —✳— 3.00 Days

Shear Stress
D50 = 4 mm.

—■— 0.00 Days —⊗— 0.75 Days —▼— 1.50 Days —△— 2.25 Days —✳— 3.00 Days

47

Figure 4. - Cross-Section Aggradation/Degradation   16

Approach Cross-Section
Station 2050 - 4 mm.

0.00 Days 0.75 Days 1.50 Days 2.25 Days 3.00 Days

Bridge - Upstream
Station 1450 - 4 mm.

0.00 Days 0.75 Days 1.50 Days 2.25 Days 3.00 Days

48

Figure 4. - Cross-Section Aggradation/Degradation (cont.)   17

Bridge - Downstream

Station 1400 - 4 mm.

Legend: 0.00 Days, 0.75 Days, 1.50 Days, 2.25 Days, 3.00 Days

Exit Cross-Section

Station 750 - 4 mm.

Legend: 0.00 Days, 0.75 Days, 1.50 Days, 2.25 Days, 3.00 Days

49

DESIGN METHODS FOR CLEAR-WATER LOCAL SCOUR AT BRIDGE PIERS

By Hani M. Noshi

ABSTRACT:

Different methods of estimating the maximum clear-water scour depth at bridge piers for cohesionless bed material, are presented in this paper. The methods were chosen to present briefly the work done in this field through the last decade. The main concern was to inspect the design methods that can account for the nonuniformity of the bed material. The maximum clear-water scour depth measured along a series of experiments conducted in Colorado State University laboratory, was then compared to the values resulted from the inspected design methods.

INTRODUCTION:

The problem of local scour around bridge piers has been studied extensively by several investigators. No single analytically derived equation is available because of the difficulties of the problem, such as combined effects of complex turbulent boundary layer, time-dependent flow pattern, and sediment transport mechanism in the scour hole. Due to the fact that many parameters affect the scour hole development, experimental studies have been conducted by considering only certain aspects of the problem and accepting the other parameters as constants. In this paper the local **clear-water** scour around a cylindrical piers is examined.

To be able to identify the clear-water scour case from the live-bed scour, two main mean flow velocity are introduced. Threshold or critical mean flow velocity U_c related to the stated sediment and channel slope. Of equal importance is the flow mean velocity U_{ca} beyond which armoring of the channel bed is impossible.

Threshold and limiting armor conditions are discussed first to clarify the concept of the clear-water scour. Three methods for estimating the maximum scour dept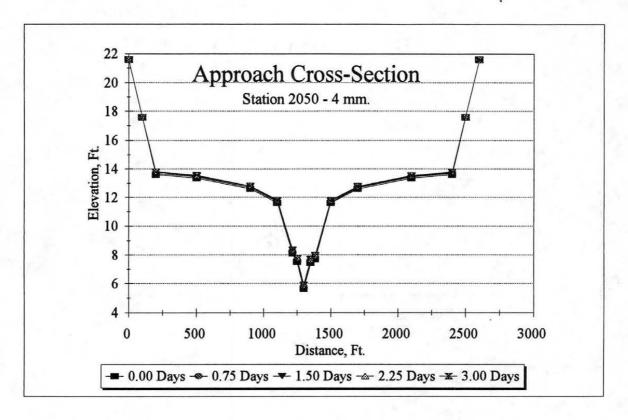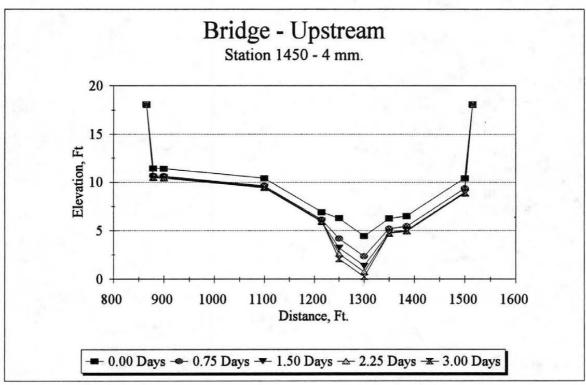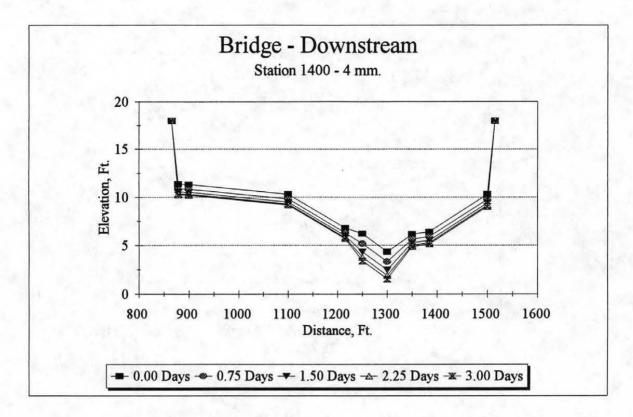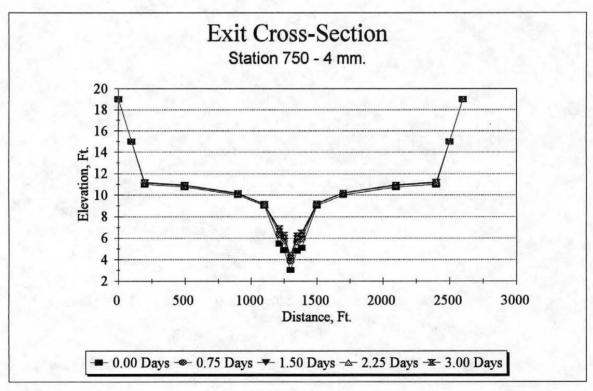h are presented. The results are then compared with the maximum scour depths around circular piers measured through set of experiments conducted at Colorado State University laboratory.

CLEAR-WATER AND LIVE BED-SCOUR:

The threshold conditions for uniform sediments is effectively determined by Shields diagram (Henderson 1966). For given fluid density and viscosity and sediment density, the Shields diagram can be used to obtain a plot of the critical shear velocity u_{*c} against grain size d_{50} as shown in Fig. 1. Water and sediment densities of 1.0 t/m^3 and 2.65 t/m^3 respectively, have been assumed in the development of Fig. 1. Threshold shear velocity is converted to threshold mean flow velocity U_c using, as an approximation, the logarithmic form of the velocity profile

x

$$\frac{U_c}{u_{*c}} = 5.75 \log(5.53 \frac{y}{d_{50}}) \qquad Eq. 1$$

where y is the flow depth. For uniform sediments, U_c will mark the transition from the clear-water to live-bed scour conditions.

For nonuniform sediments U_c will depend upon both the median grain size d_{50} and the geometric standard deviation σ_g. With nonuniform sediments, a flow can disturb the grains, removing some but simply rearranging others into an armored bed and stabilizes. For such case the flow is still considered in a clear-water stage.
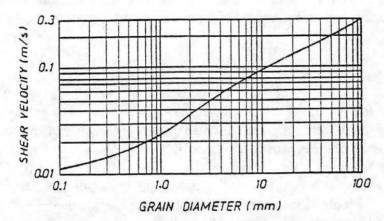
Fig. 1 Shields Chart for Threshold Condition of Uniform Sediments in Water

The flow condition beyond which armoring of a nonuniform channel bed is impossible is termed the limiting armor condition. This condition represents the coarsest or most stable armored bed for the given bed material. At flows greater than U_{ca}, no armor layer can form and the flow is then considered to be in a live-bed stage. For a given d_{50}, U_{ca} increases with increasing σ_g. Chin (1985) showed that the value of U_{ca} for a given sediment is dependent on the maximum d_{max} size and gives a method to determine U_{ca} using d_{max}, which can be found from d_{50} and σ_g if a logarithmic normal distribution is assumed:

$d_{max} = \sigma^m_g d_{50}$

Where m depends upon the size chosen for d_{max} as shown in table 1. The method of evaluation of U_a which is the appropriate flow velocity to characterize the limiting armor condition for scour determination, Baker (1986), is summarized in the flow chart of Fig. 2.

2

GRAIN SIZE DISTRIBUTION, d_{50}, σ_g, d_{max}
FLOW DEPTH, y

TABLE 1. Exponent m

Assumed value of d_{max} (1)	m (2)
d_{90}	1.28
d_{95}	1.65
d_{98}	2.06
d_{99}	2.34

Eq. 2 based on d_{50} are used herein to determine U_c for nonuniform material.

CALCULATE $d_{50a} = d_{max} / 1.8$

FIND u_{*c}, u_{*ca} from Fig. 1 using d_{50}, d_{50a}

FIND U_c, U_{ca} using u_{*c}, u_{*ca} in Eqn. 2

CALCULATE $U_a = 0.8 U_{ca}$

CHECK $U_a \geq U_c$
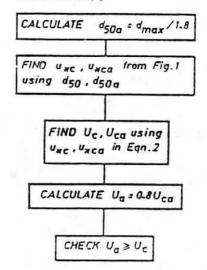
FIG. 2. Flow Chart to Calculate U_a, Limiting Armor Velocity

For nonuniform sediments, U_a is considered to mark the transition from clear-water to live-bed scour conditions.

GÜNYAKTI (1989), RAUDKIVI and ETTEMA (1983)

Through dimensional analysis, it can be observed that the relative scour depth, d_s/b, (scour depth/pier width) is a function of the relative approach depth, d_o/b, (approach flow depth/pier width) under the conditions of cohesionless uniform bed material, single pier, long flow duration, wide channel, and flow velocities close to the threshold conditions Yanmaz (1989). Breusers et al. (1977), Chiew and Melville (1987), Mellville and Sutherland (1988), Günyakti (1989), and Yanmaz (1989) present curves relating d_s/b to d_o/b. Fig. 3 shows this relation for a wide range of flow Froude numbers under live-bed and clear-water conditions for cylindrical piers. Günyakti (1989) developed the curve enveloping the data points in Fig. 3. The curve represent the upper boundary of the available scour depth data reported in the literature.

β
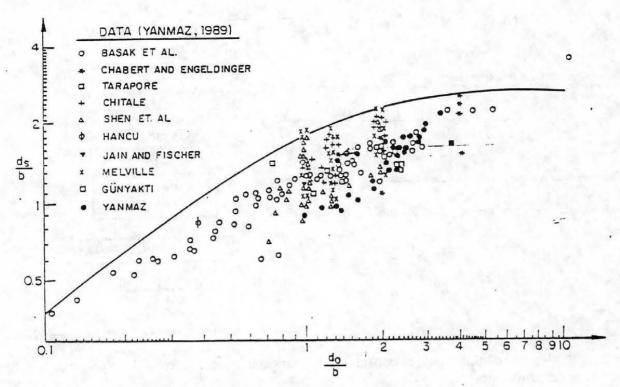
Fig. 3 Correlation between d_s/b and d_o/b for Cylindrical Piers (Yanmaz 1989)

However, the effects of sediment size and gradation can be taken into account to modify the results obtained from Fig. 3 that represents uniform materials. Raudkivi and Ettema (1983) proposed correction factors to consider the effects of sediment size Fig. 4 and the sediment gradation Fig. 5.
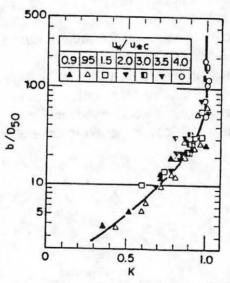
Fig. 4 Coefficient Showing Effect of Sediment Size (Raudkivi 1986)

A

53
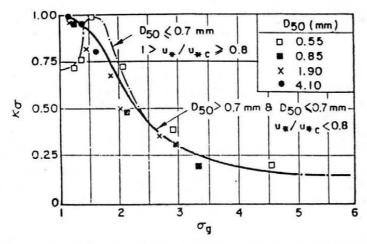
Fig. 5   Coefficient Showing Effect of Sediment Grading (Raudkivi 1986)

B. W. MELVILLE and A. J. SUTHERLAND (1988)

Equilibrium depth of local scour at a pier can be written

$$d_s = f(\rho,\nu,U,y,\rho_s,d_{50},\sigma_g,g,D,Sh,Al) \qquad Eq.\ 2$$

Where Sh and Al are parameters describing the shape and alignment of the pier. Eq. 2 can be written

$$\frac{d_s}{D} = f(\frac{UD}{\nu},\frac{U^2}{gd_{50}},\frac{y}{D},\frac{\rho_s}{\rho},\frac{d_{50}}{D},\sigma_g,Sh,Al) \qquad Eq.\ 3$$

The density ratio is assumed constant, and the Reynolds number influences are assumed negligible for the highly turbulent flows investigated. Thus,

$$\frac{d_s}{D} = f(\frac{U^2}{gd_{50}},\frac{y}{D},\frac{d_{50}}{D},\sigma_g,Sh,Al) \qquad Eq.\ 4$$

The functional relation has been evaluated using laboratory data by writing it in the form

$$\frac{d_s}{D} = K_I K_y K_d K_\sigma K_s K_\alpha \qquad Eq.\ 5$$

Where the K_I = flow intensity, K_y = flow depth ratio, K_d = sediment size, K_σ = sediment gradation, and K_s and K_α = pier shape and alignment respectively. Each parameter is now considered individually.

Flow Intensity

The flow intensity parameter determines the scouring processes that are important. The appropriate form for this parameter is
$(U-(U_a-U_c))/U_c$ for nonuniform sediment, and U/U_c for uniform sediment. For values larger than one live-bed scour occurs, while the clear-water scour pertains for values smaller than one. Fig. 5 shows the influence of flow intensity on scour depth.
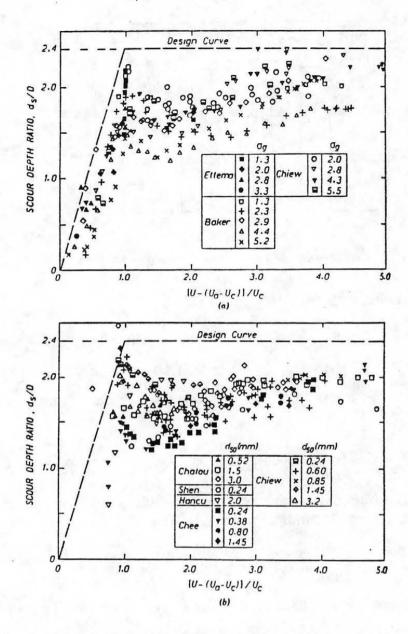
FIG. 6. Influence of Flow Intensity on Scour Depth: (a) Data by Baker (1986), Chiew (1984), and Ettema (1980); (b) Data for Uniform Sediments by Chabert and Engeldinger (1956) (Chatou Data), Chee (1982), Chiew (1984), Hancu (1971), and Shen et al. (1966)

Flow Depth Ratio

Scour depth increases with flow depth up to limiting value of the flow depth ratio y/D, beyond which there is no influence of flow depth. The flow depth factor K_y, shown in Fig. 6, is the ratio of d_s/D at a particular value of y/D to that at y/D ≥ 4. These data all have D/d_{50} ≥ 50.
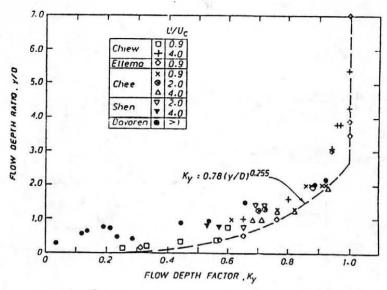
Fig. 7 Influence of Flow Depth on Scour Depth

Sediment Size Ratio

Chiew's (1984) live-bed data for uniform sediments and those of Ettema (1980) derived from clear-water flows delineate the effects of the sediment size ratio D/d_{50} on scour depth as shown in Fig. 8. K_d, the sediment size factor, is the ratio of d_s/D at a particular value of D/d_{50} to that at $D/d_{50} \geq 50$, beyond which there is no effect of sediment size.
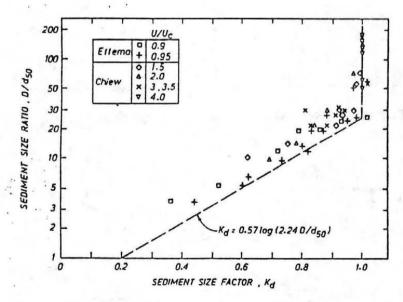
Fig. 8 Influence of Sediment Size on Scour Depth

Sediment Gradation Effects

Work by Ettema (1976) showed that the scour depths are reduced dramatically as σ_g increases, for the case of clear-water scour depths. The effects of σ_g have been largely accounted for by the introduction of U_a into the abscissa.

γ

56

Shape and Alignment Effects

Factors to account for shape are given in Table 2. These are based on aligned piers with the flow, and $K_s = 1.0$ for cylindrical piers.

TABLE 2. Pier Shape Factors, K_s

Shape in plan (1)	Length/ width (2)	Reference			
		Tison (1940) (3)	Laursen and Toch (1956) (4)	Chabert and Engeldinger (1956) (5)	Venkatadri (1965) (6)
Circular	1.0	1.0	1.0	1.0	1.0
Lenticular	2.0	—	0.97	—	—
	3.0	—	0.76	—	—
	4.0	0.67	—	0.73	—
	7.0	0.41	—	—	—
Parabolic nose	—	—	—	—	0.56
Triangular nose, 60°	—	—	—	—	0.75
Triangular nose, 90°	—	—	—	—	1.25
Elliptic	2.0	—	0.91	—	—
	3.0	—	0.83	—	—
Ogival	4.0	0.86	—	0.92	—
Joukowski	4.0	—	—	0.86	—
	4.1	0.76	—	—	—
Rectangular	2.0	—	1.11	—	—
	4.0	1.40	—	1.11	—
	6.0	—	1.11	—	—

Alignment factors K_α taken from Laursen (1958) are shown in Fig. 9.
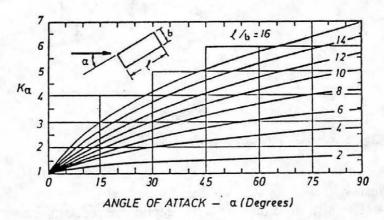
Fig. 9 Alignment Factor K_α for Piers Not Aligned with Flow

The method is summarized in flow chart form in Fig. 10.

INPUT DATA:
FLOW - y, U
SEDIMENT - d_{50}, d_{max}, σ_g
PIER GEOMETRY D, Shape, Alignment

$$\boxed{FIND\ U_c,\ U_a,\ d_{50a}\ using\ Fig.\ 2}$$

$$\boxed{CALCULATE\ \frac{U-(U_a-U_c)}{U_c}}$$

$$\boxed{\frac{U-(U_a-U_c)}{U_c} > 1}$$

No ← → Yes

$$\boxed{K_1 = 2.4\left[\frac{U-(U_a-U_c)}{U_c}\right]}\qquad \boxed{K_1 = 2.4}$$

$$\boxed{\sigma_g < 1.3}$$

No ← → Yes

$$\boxed{FIND\ K_d\ FOR\ d_{50a}\ SIZE\ USING\ Fig.\ 8}\qquad \boxed{FIND\ K_d\ FOR\ d_{50}\ SIZE\ USING\ Fig.\ 8}$$

$$\boxed{FIND\ K_y\ USING\ Fig.\ 7}$$

$$\boxed{FIND\ K_a\ USING\ Fig.\ 9}$$

$$\boxed{FIND\ K_s\ USING\ TABLE\ 2}$$

$$\boxed{d_s = K_1\ K_d\ K_y\ K_a\ K_s D}$$
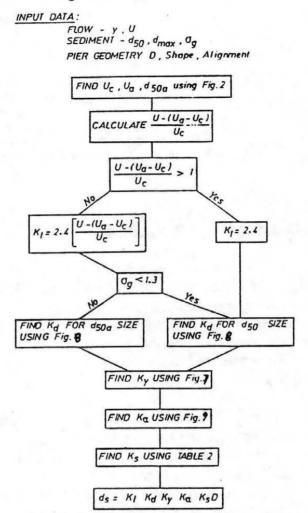
Fig. 10 Flow Chart for Determination of Design Local Scour Depth

RAUDKIVI and ETTEMA (1983)

Although many studies of local scour are reported in the literature, the number of studies dealing with the time variation of scour depth around bridge piers is very limited. Raudkivi and Ettema (1983) present sets of curves as function of σ_g that relate the relative clear-water scour depth to the nondimensional time term (u_* t/b), Strouhal number, together with the sediment based Reynolds number, and the relative sediment size on the basis of experimental studies, as shown in Fig. 10. The curves shown in Fig. 10 appear to define three straight-line segments on the semi-logarithmic plot. The first segment is associated with the rapid scouring by the down flow. The down flow excavates a groove around the perimeter of the pier. The middle segment describes the development of the scour hole as the horseshoe vortex moves away from the cylinder and grows in strength. The last segment indicates the equilibrium depth. As σ_g increases, the middle segments gradually vanish leaving only two segments.
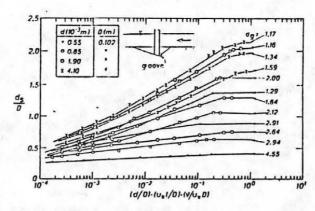
Fig. 11 –Scour Depth Divided by Pier Diameter (d_s/D) as a Function of Time in Nonuniform Bed Sediments; t = Time in Seconds; σ_g = the Geometric Standard Deviation; $d = d_{50}$; Depth of Flow = 600 mm; and u_*/u_{*c} = 0.95

EXPERIMENTAL PROCEDURE:

Experiments to study the development of scour depth around bridge pier models were conducted in a glass flume at the hydraulics laboratory of Colorado State University. The glass flume is rectangular open channel 100 cm deep, 60 cm wide. The discharge through the flume is measured by the use of water pressure manometer. Three bridge pier models made of Plexiglass were set along the flume 9.0 ft apart.

The experimental conditions that were maintained in the laboratory can be summarized as follows:

1. Only clear-water conditions with a flat bed were studied. No sediment inflow was allowed into the scour hole from upstream.
2. In order to investigate the effect of pier size, piers with   diameters 2.0, 2.0, and 2.75 inches were used.
3. In order to investigate the effect of sediment gradation, three different kinds of sands were used; all having the same median particle size of 1.8 mm with different σ_g of 1.1, 2.6, 3.5.

Table 3.0 shows a comparison between the measured equilibrium scour depth values and the estimated values using the previous methods.

TABLE 3.0

PIER DIAMET CM.	APPROA DEPTH CM.	APPROA VELOCI M./SEC.	PARTIC MEAN D MM.	PARTIC ST. DEV. CM.	MEASU SCOUR CM.	GUNYA SCOUR CM.	MELVIL SCOUR CM.	RAUDKI SCOUR CM.
5.1	7.8	0.45	1.8	1.1	7.8	9.38	8.02	11.2
5.1	8.66	0.45	1.8	2.6	4.79	4.13	4.2	5.1
5.1	7.5	0.45	1.8	3.7	3.23	2.06	0.73	2.8
7	9.72	0.29	1.8	1.1	6.55	13.65	5.93	15.4
7	8.99	0.35	1.8	2.6	4.6	5.46	3.74	7
7	7.8	0.36	1.8	3.7	3.6	2.85	0.68	3.85

CONCLUSION

Three methods of estimating the maximum equilibrium scour depth around bridge piers were examined. The methods was chosen to be able to account for the gradation effect. The three methods were applied on experimental data. The estimated maximum scour depths and the measured were then compared. The results were not of satisfactory in most of the data points that was chosen to be compared. More methods should be applied with larger number of data points to be able to decide on a more dependable estimation of the maximum clear-water scour depth.

APPENDIX I. REFERENCES

1. A. Melih Yanmaz, and H. Dogan Altinbilek, "Study of Time-Dependent Local Scour Around Bridge Piers", Journal of Hydraulic Engineering. Vol. 117, No. 10, October,1991.
2. B. W. Melville, and A. j. Sutherland, "Design Method For Local Scour At Bridge Piers", Journal of Hydraulic Engineering. Vol. 114, No. 10 October,1988.
3. Arved J. Raudkivi, and Robert Ettema, "Clear-Water Scour At Cylindrical Piers", Journal of Hydraulic Engineering, Vol. 109, No. 3, March, 1983.

APPENDIX II. NOTATION

b, D = pier width;
d_{max} = maximum particle size for a nonuniform sediment;
d_o, y = approach flow depth;
d_s = equilibrium scour depth below mean bed level;
d_{50} = median particle size;
d_{50a} = d_{50} size of the coarsest armor layer;
g = gravitational acceleration;
K_d = sediment size factor;

K_I = flow intensity factor;
K_s = pier shape factor;
K_y = flow depth factor;
K_α = pier alignment factor;
K_σ = sediment gradation factor;
Sh = effect of pier shape;
U = mean approach flow velocity;
U_a = mean approach flow velocity at the armor peak;
U_c = mean approach flow velocity at threshold condition;
U_{ca} = mean approach flow velocity beyond which armoring of channel bed is impossible;
u_{*c} = critical shear velocity;
u_{*ca} = critical shear velocity of armored bed;
v = kinematic viscosity;
ρ = fluid density;
ρ_s = sediment density; and
σ_g = geometric standard deviation of particle size distribution.

LIVE-BED SCOUR AT CYLINDRICAL BRIDGE PIERS

By Lilian Posada G.[1]

ABSTRACT :   The different approaches found in literature for designing local scour at bridge piers have been developed mostly from laboratory experiments, so it is of interest to compare field observations with the proposed criterion. A selected group of equations is analyzed in this paper to check these theoretical values against field measurements. Equations by Laursen and Toch (1956), Jain and Fisher (1979), Melville and Sutherland, (1988), Froehlich (1988), Hancu (1971), Chinese (1981) and Gao (1992) are reviewed and a comparison is presented. A comprehensive set of field data is selected from compilations reported by Froehlich (1988), Zhuravljov (1978) and Gao (1993). Due to the wide variety of flow conditions, pier shapes, and sediment gradation, available on the reported data, the analysis is made for live-bed scour around cylindrical piers with sediment sizes ranging from 0.06 mm to 20 mm.

I. INTRODUCTION

Scour is a state of non-equilibrium of sediment transport within an area or a particular region. According to Laursen (1952), the scour occurs whenever the rate of sediment transport out of an area or region exceeds the rate of supply to the area or region.

Because the forces required to erode or scour cohesive sediments are generally greater than those for noncohesive sediments with approximately the same grain size, the rate and extent of the scour depends on this property rather than on the properties of the particles. Once the individuals bonds has been broken, the particles become a part of the non-cohesive population.   Further deposition, scour or transport become a function of the properties of these separate particles.   In this paper we will refer only to non-cohesive material.

First of all, we will present a brief review of the local scour phenomena, a description of the main variables involved in the mechanism of local scour around bridge piers since most of the experimental equations that we are going to review are based upon dimensional analysis or regression analysis; then we will differentiate between clear water scour and live-bed scour to finally apply the theoretical equations for live-bed scour and compare with the field measurements.

---

[1]   Graduate Student, Colorado State University, Hydraulics Program, ERC, A115, Fort Collins, CO.

LOCAL SCOUR

Local scour is defined as the abrupt decrease in the bed elevation near an obstacle (piers, abutment, etc) due to the scour of the bed material by the very complex flow pattern induced by the obstacle. The extent of the scour hole is approximately determined by the angle of repose of the bed material and the depth of scour.

The mechanism of local scour . The nature of the flow pattern upstream and around a bridge pier has been described by Tison (1961) (Manual of Sedimentation, 1975) and more recently, a detailed description of the large scale eddy structure, the vortex system, that occurs around the pier from the free surface to the bed, is presented by Raudkivi (1986) from which figure 1 is extracted. Because of the obstruction (pier) an elevation of the water surface profile occurs in front of the pier; the induced pressure field causes a downward flow on the upstream face of the obstruction which will give rise to a separation of boundary layer at the streambed upstream of the cylinder. The horseshoe vortex forms and expands as a result of the boundary layer separation. The arms of the horseshoe vortex, extending around the circumference of the cylinder, oscillate laterally and vertically at the same frequency as the shedding wake vortices.
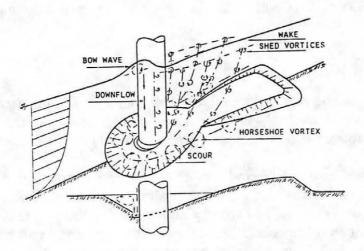
Figure 1. Flow pattern around a cylindrical pier (Raudkivi, 1986)

The wake vortex. For the stable range of flow conditions ($40 < Re_c < 150$) the Karman tail vortex were formed behind the pier. The free vortex moving downstream were decayed by viscous diffusion if no turbulence is present. In regard to the irregular range of flow conditions turbulence was developed and individual vortices were generated and initially bent by the main flow as they were convected away from the cylinder. Each vortices acts as a vacuum cleaner, picking up the material and carrying it downstream (Melville, 1988). The

Posada G.

trailing vortex is composed of one or more discrete vortex attached to the top of the pier and extending downstream.

Local scour classification . The mechanism of local scour is greatly influenced by the sediment transport characteristics of the flow. According to Laursen:
- the rate of scour will decrease as the flow section is enlarged by erosion;
- There will be a limiting extent of scour for given initial conditions, and
- The limit will be approached asymptotically with respect to time.

Clear-water scour. The sediment is removed from the scour hole and not replenished by the approach flow. The equilibrium scour depth is approached asymptotically when the flow is no longer capable of removing bed material from the scour hole. If the flow characteristics (except velocity) are kept constant, the larger the flow velocity, the larger will be the equilibrium depth. Clear water scour begins when $V/U_c < 1.0$ (Melville,1988) Froehlich pointed out that when $V/U_c < 0.5$, scour depth should be zero.

Live-bed scour. The scour hole is continually supplied with sediment by the approach flow. The equilibrium scour depth is attained when, over a period of time, the average amount of sediment transported into the scour hole by the approach flow is equal to the average amount of sediment that is removed from the scour hole due to local scour action. The local scour depth fluctuates about a mean value which is referred to as the equilibrium depth of scour. With continuous sediment motion, the equilibrium depth becomes independent of the flow velocity. Live-bed scour starts when $V/U_c > 1.0$.

Parameters influencing local scour around bridge piers. The parameters influencing local scour around bridge piers can be classified in five groups:

- Fluid characteristics. Density (ρ), kinematic viscosity (ν).
- Flow variables. Depth of approach flow (H), mean approach velocity (V), roughness of bed upstream of the pier
- Bed material variables. Grain diameter (D_{50}) and shape, grain size distribution (σ_g), density of sediments (ρ_s)
- Characteristics of the bridge pier. Pier length (L), width (B), and shape (cylindrical, round nose, rectangular, etc), surface roughness, number and spacing of the piers in the stream, angle of attack, α (orientation of pier with respect to the direction of flow), pier protection.

- Time. The depth of scour reaches a maximum at a value of the tractive force on the bed necessary for general bed material transport. For tractive forces on the bed larger than this (live-bed scour), the depth of scour varies periodically with time and about an equilibrium value due to dunes moving through the scour hole. further, the equilibrium scour depth was found to decrease slightly for tractive forces larger than the critical. Laursen and Toch observed that the equilibrium scour depth for live-bed scour was independent of velocity and sediment size. For clear water scour, the equilibrium scour depth is approached

Posada G.

asymptotically with time. Figure 2 shows the variation of local scour with time and velocity.
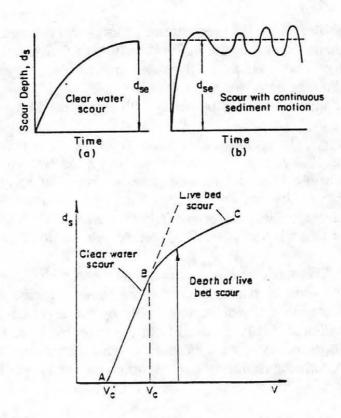
Figure 2. Variation of scour depth (a),(b) with time, (c) with velocity (Gao, 1992)

Because of the large number of variables involved and the difficulties to represent them with parameters, and to obtain real measurements of some of those variables, some assumptions have been made to approach the study of the phenomena. By evaluating the relative magnitude of some variables with respect to the others, the relevant variables are first selected. By using Dimensional analysis the selected variables are organized in non-dimensional groups (numbers)

II. ESTIMATION OF SCOUR DEPTHS

Local scour around bridge piers has been extensively studied. In this paper we refer only to those concerning to live-bed scour. Due to the many factors that control the phenomena, the number of variables have been reduced according to the observations in flume experiments, dimensional analysis, and the conditions under which those experiments were developed. Most researchers prefer to work with experiments rather than in the field because of accurate field measurements have been difficult to obtain. That is basically because of the severe 3-D flow pattern that occurs at bridges during floods, the problems and costs

Posada G.

associated with recording instruments during periods of peak flows.

To overcome this difficulty, the Ministry of Railway and Communications of China cooperated to measure the scour depth of piers in flood periods from 1958 to 1964. From these field data the expressions for critical velocity and scour depth were obtained. Gao (1989) reviewed and adjusted those equations to get the final equation that we include in this paper (Gao, 1992).

Dimensional Analysis . Relative scour depth (generally, scour depth to pier width ratio) is a function of flow variables, fluid variables, pier variables, sediment variables, and time. A general expression is :

$$D_s = f_1 \left(H, \ B, \ V, \ D_{50}, \ \sigma_g, \ \phi, \ \alpha, \ \rho_s, \ \rho, \ g, \ \nu, \ t \right)$$

$$\frac{D_s}{B} = f \left(\frac{H}{B}, \ \frac{D_{50}}{B}, \ \sigma_g, \ \phi, \ \alpha, \ \frac{Vt}{B}, \ Fr \right)$$

Critical Velocity . The computed scour depth can vary depending upon the critical velocity. The Chinese literature distinguish between the critical velocity for initiation of motion of the bed material, U_c, and the initial velocity of scour at a pier, U_c'. The latter being a fraction of the critical velocity

The critical velocity equation used in China is (Zhang Rui Jin, 1981):

$$U_c = \left(\frac{H}{D} \right)^{0.14} \left(17.6 \ \frac{\rho_s - \rho}{\rho} \ D + 0.000000605 \ \frac{10 + H}{D^{0.72}} \right)^{0.5}$$

$$U_c' = 0.645 \ U_c \left(\frac{D}{B} \right)^{0.053}$$

where D is the average diameter of bed material (m).

The critical velocity equation used by Froehlich (1988) is:

$$U_c = 1.58 \ \sqrt{(S_s - 1) \ g \ D_{50}} \ \left(\frac{H}{D_{50}} \right)^{\frac{1}{6}}$$

Melville and Sutherland (1988) use the Shields diagram to compute the critical velocity at the threshold conditions.

Posada G.

Formulation

Chinese Equations

- Gao and others, (1993):

$$D_s = 0.65 \; K_s \; H^{0.15} \; B^{0.60} \; D^{-0.07} \left(\frac{V - U_c'}{U_c - U_c'} \right)^n$$

$$n = \left(\frac{U_c}{V} \right)^{9.35 \, + \, 2.23 \log D}$$

$$U_c' = 0.645 \; U_c \; \left(\frac{D}{B} \right)^{0.053}$$

American and Australian Equations

- Neill (1964) about Laursen and Toch (1956):

$$D_s = 1.35 \; B^{0.7} \; H^{0.3}$$

- Hancu (1971), in Breuser and others (1977):

$$D_s = 2.42 \; B \; f\left(\frac{V}{U_c} \right) \left(\frac{U_c}{g \, B} \right)^{\frac{1}{3}}$$

$$f\left(\frac{V}{U_c} \right) = 0 \qquad\qquad for \; \left(\frac{V}{U_c} \right) \leq 0.5$$

$$f\left(\frac{V}{U_c} \right) = 1.0 \qquad\qquad for \; \left(\frac{V}{U_c} \right) \geq 1.0$$

$$f\left(\frac{V}{U_c} \right) = \frac{2 \, V}{U_c} - 1 \qquad\qquad for \; 0.5 < \frac{V}{U_c} < 1.0$$

This equation establish a maximum limit for scour depth of 2.42 times the pier width when the approach velocity is equal to the critical velocity. This maximum value is lately confirmed by Melville and Sutherland (1988).

Posada G.

- Jain and Fisher (1979) :

$$D_s = 2.0 \ B \left(\frac{H}{B} \right)^{0.50} \left(\frac{V}{\sqrt{g\,H}} - \frac{U_c}{\sqrt{g\,H}} \right)^{0.25}$$

for live-bed scour, (Fr - Fr$_c$) > 0.2

- Froehlich (1988):

$$D_s = 0.32 \ K_1 \left(\frac{B'}{B} \right)^{0.62} \left(\frac{H}{B} \right)^{0.46} \left(\frac{V}{\sqrt{g\,H}} \right)^{0.20} \left(\frac{B}{D_{50}} \right)^{0.08}$$

- Melville and Sutherland (1988):

$$D_s = B \ K_\alpha \ K_H \ K_D \ K_\sigma \ K_s \ K_I$$

In this equation, the maximum value of D_s is equal to 2.4 times the width of the pier, which is an envelope curve drawn to the experimental data considered in the analysis.

III. ANALYSIS OF RESULTS

Characteristics of Field Data . From almost 475 field measurements of local scour around bridge piers, including different widths and shapes, a wide range of sediment sizes, flow depths, and flow velocities, a set of 40 points were selected. From the subset of cylindrical piers, those for which the relationship $V/U_c > 1.0$, when using any formula for critical velocity (the extreme cases) were selected. Finally, the set presented in Table 1 was selected trying to cover a full range of Fr numbers, but under the above conditions, the highest Fr was 0.78.

Comparison between measured and computed scour depths . Figure 3 is a dimensionless graph showing the variation of the measured scour depth (Dm/B) with respect to the computed scour depth (Ds/B). Equations by Jain and Fisher (J&F) and Laursen and Toch (L&T) overpredict the scour depth whereas Froehlich and Hancu underestimate the local scour. It is important to note that Froehlich's equation used here does not included the safety factor equal to 1.0 included for design purposes. Gao's equation seems to be around the line of perfect agreement.

Figure 4 shows the variation of the computed scour depth per unit width to the flow depth per unit width. As expected, Equation by L&T shows a clear trend since, the equation involves explicitly the factor H/B. Hancu's equation seem to behave constant with this

Posada G.

Table 1. Calculation of local scour around piers using field data

| Case Numbe	Dm (m)	B (m)	H (m)	D50 (mm)	V (m/s)	Fr	GAO Dc/B 1992	FROEH Dc/B 1988	J&F Dc/B 1979	HANCU Dc/B 1971	L&T Dc/B 1964
1	4.30	8.20	4.30	0.060	0.61	0.09	0.63	0.38	0.67	0.26	1.11
2	4.08	4.33	11.19	0.160	1.07	0.10	1.13	0.71	1.61	0.39	1.79
3	5.40	3.60	2.50	0.165	1.87	0.38	0.90	0.50	1.22	0.44	1.21
4	4.10	3.60	1.10	0.165	2.29	0.70	0.75	0.38	0.96	0.42	0.95
5	3.90	3.60	1.00	0.165	1.89	0.60	0.76	0.36	0.87	0.41	0.92
6	3.20	3.60	0.90	0.165	1.36	0.46	0.79	0.32	0.75	0.41	0.89
7	5.50	3.05	4.20	0.200	2.20	0.34	0.90	0.65	1.71	0.43	1.49
8	5.20	3.05	4.00	0.200	2.72	0.43	0.86	0.66	1.79	0.43	1.46
9	5.00	3.05	5.00	0.200	2.48	0.35	0.91	0.71	1.89	0.43	1.57
10	4.40	3.05	2.40	0.200	1.32	0.27	0.89	0.48	1.18	0.41	1.26
11	4.36	4.30	9.99	0.200	0.95	0.10	1.01	0.66	1.46	0.40	1.74
12	3.30	3.05	10.80	0.200	2.09	0.20	1.09	0.90	2.38	0.45	1.97
13	2.20	3.05	2.00	0.200	1.84	0.42	0.81	0.48	1.23	0.41	1.19
14	5.72	4.83	17.10	0.250	1.59	0.12	0.93	0.83	2.04	0.41	1.97
15	4.50	4.90	14.50	0.250	0.69	0.06	0.85	0.66	1.27	0.40	1.87
16	1.72	4.26	9.89	0.270	1.07	0.11	0.91	0.66	1.53	0.41	1.74
17	2.30	10.20	5.80	0.300	0.60	0.08	0.55	0.34	0.57	0.30	1.14
18	4.16	4.45	11.53	0.310	1.10	0.10	0.88	0.68	1.59	0.42	1.80
19	0.61	0.50	0.79	0.320	0.61	0.22	1.44	0.53	1.36	0.74	1.55
20	1.74	4.50	13.08	0.340	1.20	0.11	0.86	0.71	1.71	0.42	1.86
21	4.70	5.03	15.40	0.350	1.47	0.12	0.81	0.75	1.86	0.41	1.89
22	0.31	0.25	0.40	0.360	0.39	0.20	1.61	0.49	0.96	0.90	1.56
23	0.40	0.40	0.53	0.380	0.43	0.19	1.39	0.46	0.94	0.79	1.47
24	0.33	0.20	1.08	0.380	0.66	0.20	2.10	0.83	2.48	1.04	2.24
25	0.46	0.40	1.40	0.400	0.62	0.17	1.64	0.69	1.83	0.85	1.97
26	0.31	0.20	1.15	0.410	0.66	0.20	2.08	0.85	2.53	1.05	2.28
27	2.55	4.50	12.18	0.420	1.14	0.10	0.81	0.68	1.62	0.43	1.82
28	3.65	4.40	11.39	0.440	1.09	0.10	0.81	0.66	1.57	0.43	1.80
29	2.84	2.87	5.14	0.520	1.23	0.17	0.78	0.59	1.55	0.46	1.61
30	2.41	4.10	9.34	0.600	0.93	0.10	0.77	0.59	1.36	0.46	1.73
31	7.80	8.50	9.00	0.670	0.65	0.07	0.53	0.41	0.67	0.37	1.37
32	3.00	4.30	10.59	0.880	1.12	0.11	0.71	0.61	1.47	0.51	1.77
33	3.98	4.21	5.60	1.000	0.95	0.13	0.65	0.47	1.06	0.51	1.47
34	4.80	5.00	16.55	1.530	1.57	0.12	0.65	0.70	1.81	0.57	1.93
35	1.22	1.52	3.20	1.600	1.98	0.35	0.75	0.63	2.01	0.77	1.69
36	0.90	0.98	1.70	8.000	1.61	0.39	0.76	0.50	1.07	1.49	1.59
37	1.30	1.50	3.10	20.000	2.38	0.43	0.65	0.53	1.10	1.70	1.68
38	0.80	1.50	2.50	20.000	2.54	0.51	0.61	0.50	1.33	1.67	1.57
39	0.50	1.50	0.90	20.000	2.33	0.78	0.52	0.34	0.98	1.49	1.16
40	0.40	1.50	1.30	20.000	2.68	0.75	0.54	0.40	1.24	1.55	1.29

8
69

Posada G.
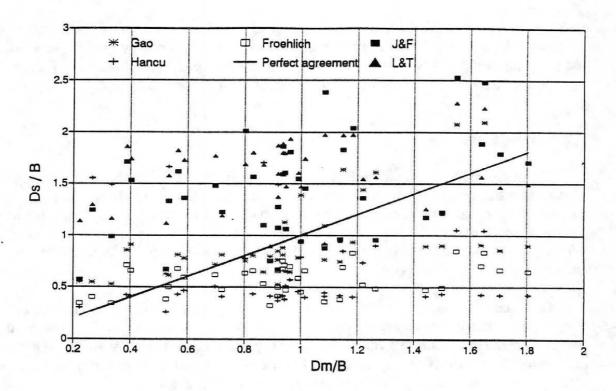
Figure 3. Comparison of measured and computed local scour depths.
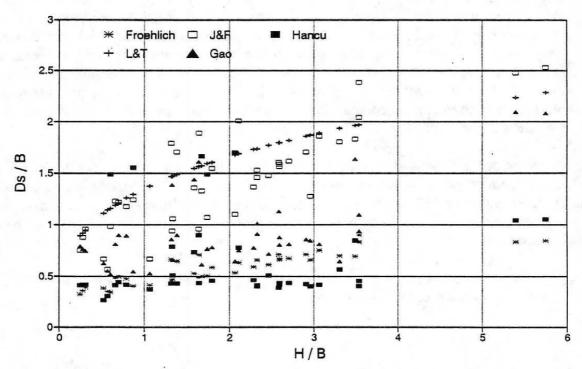

Figure 4. Variation of local scour per unit width with flow depth per unit width.

Posada G.

70

relationship (H/B); Froehlich, Gao and J&F equations shows a trend of increasing scour depth as the depth increases. The more dispersion in that trend is shown by the J&F method. The equation proposed by Melville and Sutherland is, for the conditions of the data analyzed here, a constant line at Ds/B = 2.4 which is the upper limit of the scour depth.

IV. CONCLUSIONS

The measured local scour depth is a result of scour due to modification of the flow (river contraction because of the abutments and piers, accumulation of debris and ice, etc), natural scour due to degradation of the streambed. The computed scour depth only takes into account the local scour due to the perturbation of the flow around the pier; so, the measured scour should always be greater than the computed. In this sense, Hancu equation underestimates in more degree the scour depth.

The maximum value of scour depth, as reported by Melville and Sutherland, and verified for most of the american equations, is 2.4 times the pier width (a limit based on the experimental data). During a flood, the scour depth can be measured relatively easily but the associated flow velocity and the sediment size are very difficult to measure; then, the reported conditions during floods are very uncertain, specially V and D_{50}.

Also, large sediment sizes in the bed material can distort the depth of the scour, creating some turbulence around the particle by which the velocity and pressure conditions are altered with respect to the flume conditions The variation of scour depth with respect to the mean diameter showed a rather scatter plot; high concentration of fine sediments could modify the flow and fluid characteristics; several equations has been proposed to account for the velocity at the threshold conditions when the sediment initiates its movement, and they can make a difference when the sediment gradation is wide. Those are some of the possible reasons for what the measured and the computed scour depth are different, and most important of all, the measured scour depth is greater than the 2.4 B limit.

None of the flows had high Froude numbers, and Jain and Fischer (1979) found ratios of scour depth to pier diameter greater than 2.4 for some Froude numbers greater than one. High Froude numbers are fairly common during floods in streams of arid and semi-arid regions, so the question of whether or not the proposed design equation applies to these cases is important.

In this connection, it would be of interest to know the range of Froude numbers for the experimental data used by the authors in their development.

Posada G.

APPENDIX I. REFERENCES

Breusers, H.N.C., Nicollet, G., and Shen, H.W., 1977. " Local scour around cylindrical piers". Journal of Hydraulic Research, 15(3), 211-252.

Froehlich, D. C., 1988. "Analysis of onsite measurements of scour at piers." Hydraulic Engineering, Proceedings of the 1988 National Conference, Hydraulics Div., ASCE, 534-539.

Jain, S.C., and Fischer, E.E., 1979, Scour around circular bridge piers at high Froude numbers, U.S. Department of Transportation, Federal Highway Administration Report no. FHWA-RD-79-104, 65 p.

Laursen, E.M., and Toch, Arthur, 1956, Scour around bridge piers and abutments, Bull. no. 4, Iowa Highway Research Board, 60 p.

Melville, B.W., and Sutherland, A.J., 1988, Design method for local scour at bridge piers, American Society of Civil Engineers, Journal Hydraulic Engineering, Vol. 114, no. 10, p. 1210-1226.

Neill, C.R., 1964, River-Bed Scour, A review of Bridge Engineers, Canadian Good Roads Assoc. tech. pub. # 23, Ottawa, Canada, 37 p.

Raudkivi, A.J., 1986, Functional trends of Scour at Bridge Piers, Journal of Hydraulic Engineering, Vol 112, No.1. ASCE, 1-13.

Richardson, E. V., and others, 1975. "Highways in the river environment, hydraulic and environmental design considerations.", U.S. Department of Transportation, Federal Highway Administration.

Zhuravljov, K. T. (1978). "New method for estimation of local scour due to bridge piers and its substantiation." Trans. 109, Ministry of Transport Construction. State all Union Scientific Research Institute on Roads, Moscow (translation from Russian).

APPENDIX II. NOTATION

The following symbols are used in this paper (SI system of units is used):

α = Angle of attack
B = Pier width
B' = B cos α + L sin α
D_m = Measured scour depth
D_s = Computed scour depth (m)

II 72   Posada G.

D_{50} = Median size of bed sediments
Fr = Froude Number
g = gravity
H = Flow depth
K_I = Flow intensity factor
K_H = Flow depth factor
K_D = Sediment size factor
K_σ = Sediment gradation factor
K_s = Pier shape factor
K_α = Pier alignment factor
L = pier length
Re_c = Reynolds number associated to the pier width.
Ss = Specific gravity of sediments
U_{*c} = Threshold shear velocity
U_c = Mean approach flow velocity at threshold conditions
U'_c = Critical velocity for initiation of scour depth
V = Approach velocity of flow

Posada G.

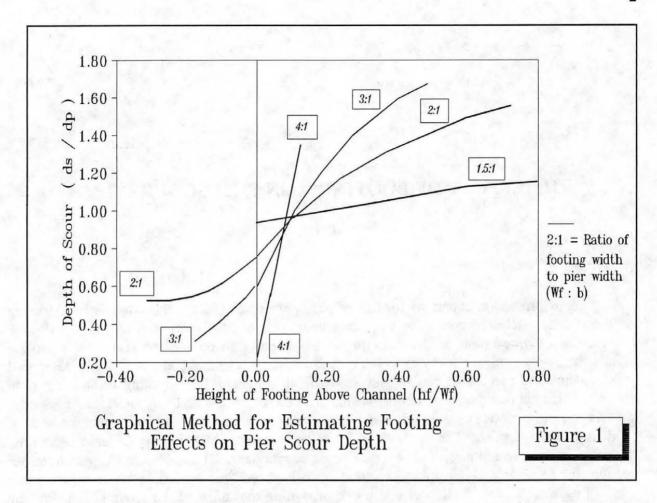# THE EFFECT OF FOOTINGS ON PIER SCOUR DEPTH

Lisa M. Fotherby

Abstract

Scour prediction equations for bridge piers rarely account for the effects of the footing on the resulting scour depth. The Chinese equations and three indirect techniques: the 10% switch, the weighted pier, and the dominant component, can be used to account for footing effects, but, only consider footings which extend above the channel bed. A recently developed graphical method can adjust bridge pier scour depth estimates for a footing located not only above the channel bed, but also, below the channel bed, or level with the channel. In this study, six sets of field data from pier/footing combinations were used to compare different methods of predicting scour depths. The methods included the graphical method, the Chinese equations, the three indirect techniques, and two pier scour equations, CSU and Froehlich, which do not account for footings. The graphical method performed well for predicting scour depths when the footing was located at channel bed level, or, within the range of the scour hole below the channel bed. The field data in this study was insufficient to adequately compare the methods which applied to the condition of a footing extending above the channel bed.

Introduction

Many empirical equations have been developed to estimate the scour depth at a bridge pier. In the majority of these equations, no consideration is given as to how a footing will influence the scour hole. One exception is the Chinese equations. A shape factor is included in the Chinese equations to account for footings extending into the flow field. The Chinese equations, however, were not available in english until very recently. Instead, in the U.S., several indirect techniques evolved to account for the influences from a footing. In these techniques, the pier width parameter found in most scour depth equations, is modified. The indirect techniques and the Chinese equations focus exclusively on sites where the footing extends above the channel bed.

Two laboratory flume studies in 1990 and 1991, conducted at the Federal Highway Administration Research Center, in MacLean Virginia, focussed on how a footing would effect

Graphical Method for Estimating Footing Effects on Pier Scour Depth

Figure 1

the depth of scour. As part of the study a literature search was also conducted on previous laboratory flume testing of footing/pier combinations. A graph was developed from the combined data (see Figure 1). The graph indicates the percent of adjustment which should be made to estimated pier scour depth values if a footing is present (Fotherby, 1992, Fotherby and Jones, 1993).

The objective of this study is to use published scour field data from pier/footing combinations to compare the accuracy of the graphical method, the Chinese equations, and the indirect techniques of accounting for footing effects. The graphical method differs from the Chinese equations and indirect techniques because it is also capable of predicting footing effects when a footing is level with the channel bed, or, installed lower than the channel bed.

The Equations

Three equations are employed in this comparison; the Chinese equations from 1964 (Dongguang, Posada, and Nordin, translated 1993), the CSU equation from 1975 (Richardson, Simons, Julien, 1990), and the Froehlich equation from 1988 (Froehlich, 1991). The Chinese equations are the only equations known to account directly for footing effects. A shape factor

in the Chinese equations is specified by the size and the location of the footing above the channel bed. Several charts which cover an assortment of pier and footing shapes, were developed for the Chinese equations to help select the shape factor. A limitation of the equations is that they do not consider footing influences when the footing is level with the channel bed or lower than the channel bed. The Chinese equation for live bed scour is:

$$d_s = 0.46 \ K \ B_1^{0.60} \ y_o^{0.15} \ D_{50}^{-0.07} \left[\frac{V_o - v_c'}{V_c - v_c'} \right]^n$$

$$where \qquad n = \left[\frac{V_c}{V_o} \right]^{9.35+2.23 \log D_{50}} \tag{1}$$

$$v_c = \left[\frac{y_o}{D_{50}} \right]^{0.14} \left[17.6 \ \frac{\rho_s - \rho}{\rho} \ D_{50} + (6.05*10^{-7}) \frac{10 + y_o}{D_{50}^{0.72}} \right]^{0.5}$$

$$v_c' = 0.645 \left[\frac{D_{50}}{B_1} \right]^{0.053} v_c$$

The CSU equation was developed at Colorado State University and is recommended by the Federal Highway Administration in Hydraulic Engineering Circular No. 18 (1988). The equation was empirically developed from laboratory flume studies and is easy to apply. It does not include a parameter to account for footings, nor a parameter for sediment particle size. Neither of these exclusions are unusual. The author has been unable to note any equation other than the Chinese equation which accounts directly for footings, and approximately half or more of the available scour depth prediction equations do not include a parameter for sediment size. The CSU equation is shown below.

$$\frac{d_s}{y_o} = 2.0 \ K_1 \ K_2 \left[\frac{b}{y_o} \right]^{0.65} Fr^{0.43}$$

$$where \qquad Fr = \frac{V_o}{(g \ y_o)^{0.5}} \tag{2}$$
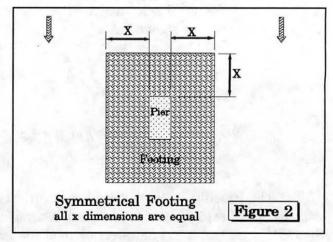
The Froehlich equation is also empirical in nature, but, it was developed from 83 field data sets at 23 bridge sites. The equation contains a parameter for sediment size, although, like the CSU equation, it has no direct method for accounting for pier/footing combinations. When Froehlich developed his equation he adjusted his input data from sites with a pier/footing combination by entering the footing width as b, rather than the pier width. Three of the bridge sites used to develop Froehlichs' equation are also used as data sets in this comparison.

Froehlichs' equation is:

$$\frac{d_s}{b} = 0.32 \ K_3 \left[\frac{B_3}{b}\right]^{0.62} \left[\frac{y_o}{b}\right]^{0.46} Fr^{0.20} \left[\frac{b}{D_{50}}\right]^{0.08} + 1.0 \qquad (3)$$

Froehlich added the value, 1.0, on the end of his equation as a factor of safety. The factor of safety was not used in this study because a prediction value, rather than a conservative design value, was sought.

In addition to the Chinese, CSU, and Froehlich equations, three indirect techniques are also considered. The indirect techniques account for footing effects by modifying the pier width parameter, b, in existing scour depth equations. The three indirect techniques are; the 10% depth switch, the weighted pier width, and the dominant component (Jones, 1992). The 10% depth switch technique suggests the use of footing width rather than pier width in scour depth equations, when the footing extends more than 10% into the flow field. The weighted pier technique employs a weighted average of pier and footing widths in scour depth equations based on the length of the pier and the footing exposed to the flow field. The dominant component technique requires two scour calculations and recommends the use of the calculation which produces the most scour. The first calculation considers scour depth of the footing alone using a velocity at the height of the footing. The second calculation considers scour depth from the pier alone using the approach velocity. All three techniques; the 10% switch, weighted pier, and dominant component, address footing effects only when the footing extends above the bed of the channel. The dominant component technique can be applied to any scour depth equations which contain the parameters, pier width and approach velocity; and the 10% depth switch and weighted pier techniques can be applied to any scour depth equation where pier width is a parameter. The three indirect techniques are applied in conjunction with the CSU equation and the Froehlich equation in this study.

The three scour depth equations and three indirect techniques were compared (when applicable) to the graphical method shown in Figure 1. In the graphical method, scour depth for a pier/footing combination is found by multiplying pier scour depth, calculated in any equation, by the percent indicated on the graph ($d_p * \% = d_s$). The CSU equation and the Froehlich equation are used in this study to calculate the pier scour depth (d_p). The graphical method is the only technique which accounts for footing effects when the footing is level with the channel bed

Symmetrical Footing
all x dimensions are equal   Figure 2

($h_f/W_f = 0$), or, is installed below the channel bed within the region effected by the pier scour hole ($h_f/W_f < 0$). A disadvantage of the graphical method is that it is only as accurate as the pier scour equation with which it is paired. A second disadvantage is that the method only

applies to symmetrical footings. A symmetrical footing is defined as a footing where the horizontal distance from the pier to the edge of the footing, is equivalent on the sides and the nose of the pier (see Figure 2). Table 1 contains a matrix of the equations and techniques compared in this study.

TABLE 1 - TECHNIQUES FOR EVALUATING FOOTING SCOUR EFFECTS

CSU Equation	Froehlich Equation	Chinese Equation[b]
CSU Eq. with Graphical Method	Froehlich Eq. with Graphical Method	
CSU Eq. with 10% Switch[a]	Froehlich Eq. with 10% Switch	
CSU Eq. with Weighted Pier[a]	Froehlich Eq. with Weighted Pier[a]	
CSU Eq. with Dominant Component[a]	Froehlich Eq. with Dominant Component[a]	

[a] Can only apply this technique when the footing extends above the channel bed.
[b] Provides adjustment factors for footings only when the footing extends above the channel bed.

The Data

Published field data was required to make a comparison between the techniques and methods listed in Table 1. It was difficult to locate the necessary data. A majority of published data is lacking essential elements in the description such as structure dimensions, stream flow and velocity records, or sediment particle sizes. The 83 data sets used by Froehlich in developing his empirical equation, comprise the bulk of available, complete, field scour data. Unfortunately, a high percentage of the 83 data sets used by Froehlich, do not involve shallow footings that effect scour depth. Most footings are safely installed below the influence of pier scour. One final restriction encountered while locating field data was that only symmetrical footings could be used for the graphical method. Six data sets from five bridge sites were finally located which met the required criteria. Three of the data sets were used by Froehlich to develop his equation. Of the six data sets, three sets of data
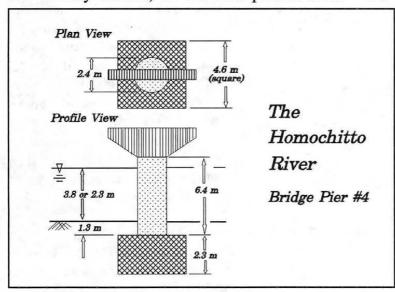
Figure 3a

Plan View
2.4 m
4.6 m (square)

Profile View
3.8 or 2.3 m
6.4 m
1.3 m
2.3 m

The Homochitto River

Bridge Pier #4

applied to sites where the footings were installed slightly below channel bed level, one set applied to a footing installed at bed level, and two sets applied to sites where the footing extended above the channel bed into the flow field. The following paragraphs contain a brief description of the five bridge sites.

Two sets of data are from the Homochitto river in Mississippi (Hopkins, Vance, and Kasraie, 1980). The U.S. Highway 84 Bridge over the Homochitto River is located 0.8 miles east of Ediceton, Mississippi. The bridge is 171 meters long and contains six piers. The main channel passes between pier 3 and pier 5. Pier 4 of the bridge was instrumented with an echo depth finder and a stage recorder to gather scour data. A discharge rating curve was supplied for the site along with a grain size analysis which indicated a d_{50} of 7.5 mm. The bed material was described as coarse sands and gravel. Figure 3a shows the dimensions of pier 4 of the U.S. Hwy 84 bridge, and the water surface and bed elevation. The footing of the Homochitto site was located 1.3 m below channel bed level. The first set of data was recorded at this site for a flood event on December 20 to 22, 1972. The high flow event produced an average sustained peak of 503 cms (17,750 cfs). The second high flow event on April 24 to 26, 1973, produced an average sustained peak flow of 208 cms (7,350 cfs).
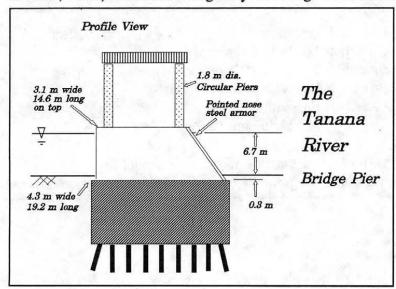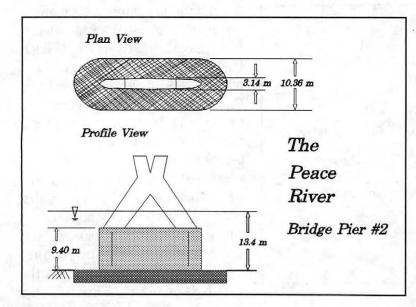
The third data set was measured on the Tanana River at Nenana, Alaska (Norman, 1975). Bridge 202 of the Anchorage-Fairbanks highway, is 152 m long with a single, centered, pier support. Figure 3b illustrates the

Figure 3b

Figure 3c

dimensions of the pier and footing. Angle of attack at this pier was 5° during collection of the data. The Tanana is a meandering glacial river with bed sediment of sand to coarse gravel. The d_{50} was listed as 15 mm. Scour depth measurements were recorded during high flow events using a boat and fathometer. The maximum approach velocity and depth occurred on August 17, 1967. The footing location for this site was 0.3 m below channel bed level.

The fourth data set was measured on the Peace River near Fort Vermilion, Alberta (Harrington and McLean, 1984). The Peace River bridge is located approximately 560 km north of Edmonton. The 532 m bridge was constructed in 1971 and a number of channel surveys were carried out at different discharges for a study to evaluate scour depth equations. The footing of the study pier at the Peace River site is located level with the bed of the channel. The Peace River is described as the largest sand bed river in Alberta and d_{50} is 0.3 mm. Figure 3c illustrates the dimensions of the study pier. Measurements at this site were made for average flow events rather then peak flow events as in the Homochitto River site and the Tanana River site. The data for this set was measured in 1972.
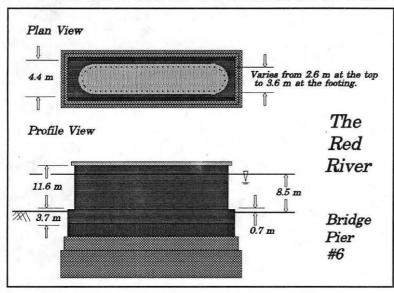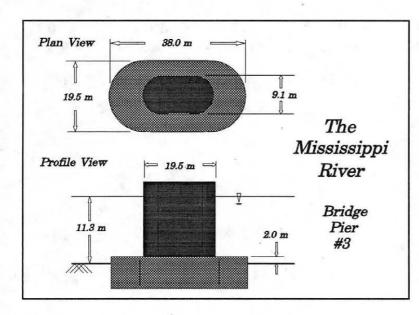
The fifth data set was measured at the Texas Street Bridge over the Red River, LA-6 at Shreveport, Louisiana (Hopkins, et al, 1980). The bridge is 945 meters long and supported by ten piers. Two piers, #5, and #6, stand in the main flow. Pier and footing dimensions and bed elevations are shown in Figure 3d. The river bed was composed of a fine sand with a d_{50} of 0.11 mm. Scour depth measurements were gathered

Figure 3d

Figure 3e

TABLE 2 - SCOUR DEPTH FIELD DATA

	Homochitto River		Tanana River	Peace River	Red River	Miss. River
y_o approach depth (m)	3.81	2.26	6.71	13.4	8.5	11.3
v_o approach velocity (mps)	2.47	2.91	2.59	2.23	0.63	0.66
d_{50} (mm)	7.5	7.5	15	0.31	0.11	0.036
b width of pier (m)	2.44	2.44	3.05	3.14	3.23	9.1
α angle of attack (°)	0	0	5	0	0	15
L length of pier (m)			16.3			19.5
K shape coefficient	1.0 Circ[a]	1.0 Circ[a]	0.9 Sharp	0.9 Sharp	1.0 Rdd[b]	1.0 Rdd[b]
W_f width of footing (m)	4.57	4.57	4.27	10.36	4.39	19.5
h_f height of ftg above channel bed (m)	-1.3	-1.3	-0.3	0.0	0.7	2.0
d_m measured scour depth (m)	0.6	0.9	1.8	2.5	2.1	10.4

[a] Circular shaped pier
[b] Round nose pier

with a depth echo sounder mounted on pier 6. The system was similar to the one used on the Homochitto River as both sites were part of the same study. Data was collected for a high flow event on December 18, 1972.

The final data set came from the Mississippi River at US-190 in Baton Rouge, Louisiana (Chang, 1980). The bridge was one km in length, supported by six round-nose piers. Two of the piers were in the flow. A sharp bend, above the bridge, created a skew at the pier of $15°$. Data at this site was collected by a Louisiana Department of Transportation hydrologic survey team as part of a routine bridge inspection program. Scour depths and channel cross sections were gathered with a boat and fathometer during normal flow periods. The bed material at the site is silty loam with a d_{50} of .036 mm. Figure 3e contains a rough representation of the pier and footing shape.

Results and Discussion

The six data sets used in this comparison are listed in Table 2. Scour depths were calculated from the data for the matrix of methods shown in Table 1. The graphical method was applied to both the CSU and the Froehlich equations for all sites. The three indirect techniques; the 10% switch, the weighted pier width, and, the dominant component, were applied to the CSU and Froehlich equations at the Red River and Mississippi River sites. The Red River and Mississippi River sites were the only sites where the footing extended above the channel bed. The data sets cover a reasonable range of variables. Sediments varied from a silty loam, $d_{50} = 0.036$ mm, to a sand and gravel, $d_{50} = 15$ mm. Flow depths varied from 2 m to 13 m. The footing width to pier width ratio went from 1.4:1 to 3.3:1, and the height of the footing above the channel bed ranged from -1.32 m to 2.0 m. Geographical locations included Alaska, Alberta, Louisiana, and Mississippi.

The results of scour depth calculations for the six data sets are compared to the measured scour depths in Table 3. The method or technique which came closest to predicting the measured scour depth is indicated by shading in Table 3. The Froehlich equation gave a closer prediction of scour hole depth than the CSU equation in five out of six data sets. One possible explanation for this performance is that three of the 23 bridge sites used to develop the Froehlich equation, were used in this comparison. The graphical method in conjunction with the Froehlich equation produced the closest value to the measured scour depth for the first set of Homochitto River data and the Red River data. The graphical method was successfully applied to the CSU equation for the Peace River data. It is interesting to note that the sediment in the Peace River is a d_{50} of 0.31 mm. The CSU equation does not include a parameter for sediment particle size, but, the equation was developed from laboratory flume tests where sand particles with a d_{50} of 0.2 to 0.6 mm are commonly used. The Peace River sediment is similar to laboratory flume sediment. The CSU predicted scour depth was also more accurate for the Red River data set in comparison to CSU predictions for the remaining four data sets. The Red River has a fine sand of $d_{50} = 0.11$ mm, which is also similar to the size of laboratory flume sand.

TABLE 3 - COMPARISON OF CALCULATED VERSUS MEASURED SCOUR DEPTHS

The Homochitto River	(12-21-72)		w/ Graphical	Measured	Chinese
h_f = -1.3 m d_{50} = 7.5 mm W_f:p = 1.9:1	CSU	3.9 m	2.0 m	0.8 m	1.4 m
	Froehlich	1.3 m	0.7 m		

The Homochitto River	(4-25-73)		w/ Graphical	Measured	Chinese
	CSU	3.9 m	2.0 m	0.9 m	1.3 m
	Froehlich	1.1 m	0.6 m		

The Tanana River	(7-30-67)		w/ Graphical	Measured	Chinese
h_f = -0.3 m d_{50} = 15 mm W_f:p = 1.4:1	CSU	5.4 m	5.0 m	1.8 m	1.9 m
	Froehlich	2.2 m	2.0 m		

The Peace River	(?-?-76)		w/ Graphical	Measured	Chinese
h_f = 0.0 m d_{50} = 0.31 mm W_f:p = 3.3:1	CSU	4.6 m	2.3 m	2.5 m	2.9 m
	Froehlich	2.1 m	1.0 m		

The Red River (12-18-72)		w/ graph.	w/ 10% Depth Switch	w/ Wghtd Pier	w/ Dom. Comp.	Measured	Chinese
h_f = 0.7 m d_{50} = 0.11 mm W_f:p = 1.4:1	CSU	2.9 m	2.8 m	2.9 m	2.9 m	2.9 m	2.1 m	3.3 m
	Froeh.	2.2 m	2.1 m	2.2 m	2.2 m	2.2 m		

The Mississippi River (6-14-77)		w/ graph.	w/ 10% Depth Switch	w/ Wghtd Pier	w/ Dom. Comp.	Measured	Chinese
h_f = 2.0 m d_{50} = 0.036mm W_f:p = 2.1:1	CSU	7.1 m	6.4 m	11.4 m	7.9 m	8.5 m	10.4 m	5.0 m
	Froeh.	6.5 m	5.9 m	10.2 m	7.2 m	6.5 m		

The Froehlich equation was most accurate for the second set of Homochitto River data and the Chinese equation was most accurate for the Tanana River data. In both instances, the graphical method applied to the Froehlich equation was the second closest scour depth predictor.

The 10% switch technique was the most accurate predictor for the Mississippi River data. However, the measured scour depth for this data set looks suspiciously high for the parameters reported. The prediction methods which performed reasonably in the previous five data sets, cluster around a value of 6.2 m, while the measured scour depth is reported as 10.4 m, 67% higher than the average value. A possible explanation for the wide variance might be an error in the measurement of the angle of attack. The angle of attack value was estimated from the position of the scour hole. If the estimated angle was low, this would explain the low values of scour depth predicted by the equations.

The 10% switch, weighted pier, dominant component, and Chinese equation, calculate footing effects when the footing is raised above the channel bed. Only two of the six data sets represented a footing located above the channel bed, and one of the data sets appears unreliable. Therefore, this study could not provide an adequate comparison between the methods. The study did, however, indicate that the graphical method was successful for scour depth estimates when the footing was located below or near bed level. No methods previous to the graphical method, had accounted for scour effects when the footing was located in this region.

Conclusions

Early scour equations did not consider footing effects when calculating scour depths. The Chinese scour depth equations appear to be one of the earliest attempts to account for footing effects on scour depth, and, the only method to date to include footing effects directly in the scour depth equation. The 10% switch, weighted pier, and dominant component techniques emerged as indirect methods to reflect footing affects through an adjusted pier width value. The Chinese equations and the indirect techniques, however, only considered footing effects when the footing extends above the channel bed. A recently developed graphical method also accounts for footing effects when the footing extends below the channel bed, or is located level with the channel bed. The following points emerged from this comparison of field measured scour depths with predicted scour depth values using the techniques listed in Table 1.

1. Footing effects can be significant and should be accounted for when estimating scour depths.
2. The graphical method is only as accurate as the scour depth equation it is used in conjunction with.
3. The graphical method accounts for the widest range of footing locations; below the channel bed, at bed level, and extending above the channel bed, but, it is limited to applications where the footing is symmetrical (see Figure 2).
4. The graphical method, developed from laboratory flume results, performed well with the available field data, but, there was insufficient field data to conclusively support the

success of this method.

5. There was insufficient data for field sites where the footing extends above the channel bed to perform a reasonable comparison between the 10% switch, pier width, dominant component, Chinese methods, and the graphical method.

6. The importance of field data for verifying laboratory results is indisputable. State transportation departments have collected large volumes of scour depth data for the bridge inspection program mandated by the Federal Highway Administration. A valuable contribution to scour research would be the analysis and publication of more of this raw field data.

Appendix I. References

Chang, F.M.(1980)."Scour at Bridge Piers; Field Data From Louisiana Files." Tye Engineering Co. for the Federal Highway Administration, FHWA-RD-79-105.

Dongguang, G., Posada, L.G., and Nordin, C.F.(1993)."Pier Scour Equations Used in the People's Republic of China: Review and Summary." Unpublished Paper, Engineering Research Center, Colorado State University, Fort Collins, Colorado.

Federal Highway Administration.(1991)."Evaluating Scour at Bridges." *Hydraulic Engineering Circular No 18: FHWA-IP-90-017*, Office of Engineering, Bridge Division, Federal Highway Administration (FHWA), Washington D.C.

Fotherby, L.M.(1992)."Footings, Mats, Grout Bags, and Tetrapods; Protection Methods Against Local Scour at Bridge Piers." M.S. thesis, Colorado State University, Fort Collins, Colorado.

Fotherby, L.M., Jones, J.S.(1993)."The Influence of Exposed Footings on Pier Scour Depths." *Proc, Hydraulics Conference*, ASCE, San Francisco, California.

Froehlich, D.C.(1991)."Upper Confidence Limit of Local Pier-Scour Predictions." *Transportation Research Record No 1290: Third Bridge Engineering Conference*, Volume 2, Transportation Research Board, Denver, Colorado.

Harrington, R.A., McLean, D.G.(1984)."Field Observations of River Bed Scour on the Peace River Near Fort Vermilion, Alberta." *Canadian J. of Civ. Engrg.*, 11(4), 782-797.

Hopkins, G.R., Vance, R.W., Kasraie, B.(1980)."Scour Around Bridge Piers." *Report No FHWA-RD-79-103*, Office of Research and Development, Federal Highway Administration (FHWA), Washington, D.C.

Jones, J.S.(1992)."Effects of Footing Location on Bridge Pier Scour." *J. Hydr. Engrg.*, ASCE, 118(2), 280-289.

Norman, V.W.(1975)."Scour at Selected Bridge Sites in Alaska." *Water Resources Investigations 32-75*, U.S. Geological Survey, Anchorage, Alaska.

Richardson, E.V., Simons, D.B., Julien, P.Y.(1990)."Highways in the River Environment." U.S. Department of Transportation, Federal Highway Administration.

Appendix II. Notation

The following symbols are used in this paper:

B_1 = characteristic width of pier and footing adjusted for angle of attack, the Chinese equation;

B_3 = characteristic width of pier adjusted for angle of attack, the Froehlich equation;

b = width of pier;

d_m = measured depth of scour;

d_p = calculated depth of scour resulting from pier width;

d_s = calculated depth of scour from a pier or pier/footing combination;

Fr = Froude number;

g = acceleration due to gravity;

h_f = height of footing above channel bed;

K = coefficient for pier and footing shape, Chinese equations;

K_1 = coefficient for pier shape, CSU equation;

K_2 = coefficient for angle of attack, CSU equation;

K_3 = coefficient for pier shape, Froehlich equation;

km = kilometers;

L = length of pier;

m = meters;

mm = millimeters;

mps = meters per second;

n = a power related to the bed level, Chinese equations;

v_c = critical velocity of bed material, Chinese equations;

v_c' = initial velocity of scour at the pier, Chinese equations;

v_o = velocity of approach flow

w_f = width of footing;

y_o = depth of approach flow;

α = angle of attack;

^{o} = degrees;

ρ = density of water; and

ρ_s = density of the sediment.

STEADY UNIFORM UNDERFLOW DENSITY CURRENTS

By Ed James

ABSTRACT: Analysis of steady, uniform underflow density currents indicates that the flow characteristics can be determined from a Chezy type equation. A densimetric Froude number which includes a term for the density difference between the density current and ambient is necessary to characterize the flow. For laminar flow with a smooth and sharp interfacial boundary, the interfacial shear stress is proportional to the bed shear stress which enables the friction factor to be calculated as a function of the Reynolds number. The stability of the density current interface is a function of the Froude number. Entrainment of ambient water across the interface is generally initiated when the Froude number is unity, and the extent of entrainment increases with increased Froude number. A critical velocity with regard to the stability of the interface can be determined from the stability parameter equation. The results of the density current analysis were used to make predictions regarding the flow characteristics of density currents flowing on various slopes, densities, and Reynolds numbers. The calculated predictions will assist in determining the flow parameters for a flume study on density current flow.

INTRODUCTION

Density currents are gravity currents caused by small density differences between two or more immiscible fluids. The difference in density can be caused by salinity, temperature, or suspended sediment concentration, and the density of the flowing fluid can be lower or higher than the ambient fluid. For example, streams flowing into lakes and reservoirs can cause underflow, interflow, or overflow density currents depending upon the relative densities of the inflow and ambient water. If the inflow fluid has a lower density than the ambient water, overflow will occur, and if the inflow is denser than the ambient water, underflow will occur. Interflows may occur in a stratified ambient water body where the inflow is denser than water near the surface, but less dense than water near the bottom. In this case the density current begins as an underflow until reaching a depth of neutral buoyancy where it changes to an interflow.

In addition to density currents caused by streams flowing into reservoirs, this phenomena occurs widely in nature. Thunderstorm outfalls, cold fronts, and sea breeze fronts are density currents of cold air. Dust storms and sand storms, and snow avalanches are density currents of particles in air (Alavian et al, 1992). Density currents also occur in the deep-sea environment and are believed to be responsible for the erosion of submarine canyons on the continental shelf and deposition of submarine fans on the abyssal plain (Garcia and Parker, 1989; Kuenen, 1951; Kukushima et al., 1985; Parker et al., 1986).

This paper will examine underflow density currents as they flow in contact with an inclined bottom. Figure 1 shows the general flow zones associated with a stream with excess density entering an ambient water body of lower density. In zone 1, the relatively dense inflow enters the reservoir and plunges (zone 2) beneath the less dense ambient water. In zone 3, the underflow density current flows in contact with the inclined bottom, and it is this zone which is the subject of this paper. Zones 4 and 5 are the separation and interflow zones, respectively, which may occur in a stratified ambient, but will not be considered further in this paper.
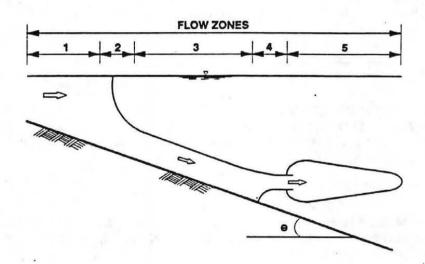
FIG. 1. Definition Sketch for Density Flow Into Stratified Ambient: Zone 1: Initial Flow; Zone 2: Plunge; Zone 3: Density Current; Zone 4: Seperation; Zone 5: interflow. (From Alavian et al., 1992)

ANALYSIS OF STEADY UNIFORM DENSITY CURRENTS

Chezy Type Equation

Middleton (1966) and Vanoni (1975) express steady, uniform density current flow in terms of a Chezy type equation

$$V = C'\sqrt{\{(\Delta\rho/\rho)dS\}} \qquad \dotfill \qquad (1)$$

where V = velocity of the uniform flow; C' = a modified Chezy coefficient; $\Delta\rho$ = the difference in density between the flow and the ambient = $\rho - \rho_a$; ρ = density of flow; ρ_a = density of ambient; d = thickness of flow; and S = slope of incline.

The main problem in predicting the average velocity of a density current is in determining the modified Chezy coefficient C'(Middleton, 1966). In open channel flow the Chezy equation is

$$V = C \sqrt{(RS)} \quad \ldots \ldots \ldots \ldots \ldots \ldots \ldots \ldots \quad (2)$$

where R = the hydraulic radius, and C is expressed as

$$C = \sqrt{(8g/f_0)} \quad \ldots \ldots \ldots \ldots \ldots \ldots \ldots \ldots \quad (3)$$

where f_0 = the Darcy-Weisbach resistance coefficient = $8(\tau_b/\rho V^2)$, and τ_b = bed shear stress.

Density current flow can also be expressed by the Chezy equation

$$V = C \sqrt{(RS)} \quad \ldots \ldots \ldots \ldots \ldots \ldots \ldots \ldots \quad (4)$$

where

$$C = \sqrt{(8(\Delta\rho/\rho)g/f)} = \sqrt{(8g'/f)} \quad \ldots \ldots \ldots \ldots \quad (5)$$

where g' = the reduced gravitational acceleration = $(\Delta\rho/\rho)g$, and f is the resistance from both the channel (f_0) and the interfacial (f_i) boundary. For a rectangular channel, R = wd/(w + 2d) and f may be written as

$$f = f_0 + [w/(w + 2d)]f_i \quad \ldots \ldots \ldots \ldots \ldots \ldots \quad (6)$$

where w = the width of the channel, and d = the thickness of the uniform underflow. For smooth straight channels, f_0 can be estimated from the Reynolds number

$$Re = Vd/\nu \quad \ldots \ldots \ldots \ldots \ldots \ldots \ldots \ldots \ldots \quad (7)$$

using a Moody diagram. The resistance at the interface (f_i) is much more difficult to predict because the interface may assume a number of different physical states as described by Middleton (1966). The possible physical states of the interfacial boundary are:

1) The interface is sharp with the underflow laminar.

2) The interface is sharp (because of the presence of a laminar boundary layer), with the underflow turbulent.

3) There are waves at the interface which travel downstream: with increasing relative motion the waves grow progressively steeper and less regular, and eventually break. Waves may be present at the interface even where the underflow is laminar.

4) There is a zone of turbulent mixing at the interface, with the underflow turbulent.

The case of a sharp interfacial boundary with a laminar underflow was considered by Vanoni (1975) in his analysis of steady uniform flows which is presented below.

Resistance Laws for Uniform Underflows

Vanoni (1975) examined the resistance laws for uniform underflows and described how variations in f with respect to Re are determined analytically for laminar flow.

A steady uniform density current will flow along an incline when the gravitational driving force is in equilibrium with the shear stresses exerted along the bed (τ_b) and along the interfacial boundary (τ_i) (Vanoni, 1975; Komar, 1971, Komar, 1977). For two dimensional flow the equilibrium equation is

$$\tau_b + \tau_i = \Delta\rho g dS \qquad \dots \dots \dots \dots \dots \dots \dots \dots (8)$$

The interfacial boundary between the flow and ambient fluid is smooth and sharp. A typical shear distribution and velocity profile for a steady, uniform density current is shown on Figure 2. Shear varies linearly from τ_b at the bottom to τ_i at the interface, and reaches zero at the point of maximum velocity. The interfacial shear is proportional to the bed shear and can be expressed as $\tau_i = \alpha\tau_b$, where α is defined as

$$\alpha = \frac{1 - 2(y_m/d)}{1 + 2(y_m/d)} = \frac{\tau_i}{\tau_b} \qquad \dots \dots \dots \dots \dots \dots (9)$$

α is also given by $\alpha = h_1/h_o$, where h_1 is the thickness of flow above the maximum velocity and h_o is the thickness of the flow below the maximum velocity. The limiting values of α are 0 for open channel flow and 1 for flow between two parallel plates. Substituting $\alpha\tau_b$ for τ_i, Eq. 1 can be rewritten as

$$\tau_b = \Delta\rho g(d/(1 + \alpha)S \qquad \dots \dots \dots \dots \dots \dots \dots (10)$$
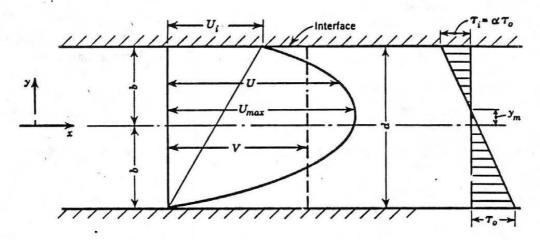

FIG. 2. Laminar Flow between Parallel Boundaries: Upper Boundary in Motion (From Vanoni, 1975)

The bed shear stress can also be expressed in terms of friction resistance by rearranging the equation for the Darcy-Weisbach resistance coefficient to

$$\tau_b = (f_0 \rho V^2/8) \quad \ldots \ldots \ldots \ldots \ldots \ldots \quad (11)$$

Combining Eqs. 10 and 11 and solving for the average velocity V yields the Chezy type equation

$$V = \sqrt{8(\Delta\rho/\rho)g/f_0} \sqrt{[d/(1 + \alpha)]S} \quad \ldots \ldots \ldots \ldots \quad (12)$$

where $d/(1 + \alpha)$ is the effective two-dimensional hydraulic radius of the density current (Vanoni, 1975).

A relationship between the friction factor f and Reynolds number was determined analytically by Vanoni (1975). The velocity profile for laminar flow can be expressed as the ratio of viscous and gravitational forces by the dimensionless parameter J, as defined by

$$J = Fr^2/ReS \quad \ldots \ldots \ldots \ldots \ldots \ldots \ldots \ldots \quad (13)$$

where Fr = the densimetric Froude number = $V/(g'd)^{1/2}$.

Vanoni (1975) established the relationship between the interface velocity (U_i) and the density currents maximum velocity (U_{max}) by differentiating the laminar velocity distribution shown on Figure 2. The result is defined by the relationship

$$\frac{U_i}{U_{max}} = \frac{12J - 1}{12J^2 + 4J + (1/3)} \quad \ldots \ldots \ldots \ldots \ldots \quad (14)$$

The J value is subject to the same limiting conditions as α. For flow between two parallel plates, $U_i = 0$, and J = 0.083 (Eq. 14). For flow in an open channel, $U_i = U_{max}$, and J = 0.333 (Eq. 14). The limiting values of J are, therefore, 0.083 and 0.333 for uniform two dimensional flow. For the usual range of densities and viscosities, U_i/U_{max} = 0.59, yielding J = 0.138 (Eq. 14) and α = 0.64 (Eq. 9) (Vanoni, 1975).

Using Eqs. 12 and 13, Vanoni (1975) was able to express the friction factor (f) as a function of the Reynolds number:

$$f = f_0(1 + \alpha) = 8/JRe \quad \ldots \ldots \ldots \ldots \ldots \ldots \quad (15)$$

where $f_0(1 + \alpha) = f_0 + f_i$.

For a laminar density current, where J = 0.138 and α = 0.64, Eq. 15 would take the form of:

$$f_0(1 + \alpha) = 1.64f_0 = 58/Re \quad \ldots \ldots \ldots \ldots \ldots \quad (16)$$

5

Eq. 16 makes it possible to calculate the value of f_0 from the Reynolds number when Re is no greater than 1000.

Substituting Eq. 16 into Eq. 12 allows the velocity of a laminar density current to be calculated as follows:

$$V = \sqrt{8(\Delta\rho/\rho)g/f_0(1 + \alpha)} \sqrt{dS} = Re^{1/2}/2.7 \sqrt{(\Delta\rho/\rho)gdS} \quad . \quad . \quad (17)$$

For a turbulent density current, the value of f_0 can be obtained from Re using a Moody diagram. However, the value of f_i is more difficult to determine. Experimental determination of α has not been sufficient to determine a relationship between α (or f_i) and Re. Experimental studies in turbulent density currents with Re values ranging from 1,000 to 25,000 indicate that the maximum velocity occurs at a depth equal to 0.7d, but no systematic variation with Re was determined (Vanoni, 1975). However, using 0.7d as the depth of maximum velocity yields $\alpha = 0.43$ (Eq. 9 or $\alpha = h_1/h_0 = 0.3/0.7 = 0.43$). Values of α ranging from 0.4 to 0.5 for Reynolds numbers up to 10^5 have been reported from analysis of experimental data for lock exchange flows (Vanoni, 1975).

Analysis of turbulent flows is made difficult because the interface becomes less distinct through mixing and the density within the flow may contain vertical variations. However, the velocity of the flow may be determined if the appropriate values of f_0 and α are used in Eq. 12.

INTERFACIAL MIXING AND STABILITY

At low velocities, the density current interface is smooth and distinct, and the density gradient across the interface is at a maximum. At increased velocities, waves begin to form on the interface, and at a critical velocity the interfacial waves will periodically break causing some mixing between the density current and the overlying ambient. Further increase in velocity cause sharp crested waves to form and an increase in the frequency of interfacial waves breaking at their crests resulting in an increase in mixing (Vanoni, 1975).

Keulegan (1949) derived a stability parameter or criterion for determining the flow conditions at which mixing across the interface is likely to occur. The stability criterion is defined by

$$\theta = \frac{(\nu g\Delta\rho/\rho)^{1/3}}{V} = \frac{1}{(Fr^2Re)^{1/3}} \quad . \quad . \quad . \quad . \quad . \quad . \quad . \quad . \quad . \quad . \quad (18)$$

θ is inversely proportional to velocity and directly proportional to the cube root of the density difference, gravity and kinematic viscosity. Velocity appears to be the controlling factor regarding the stability of the interface. Density currents with low velocities will have higher values of θ and the interface will be more stable

than density currents with high velocities. Increases in the kinematic viscosity and $\Delta\rho/\rho$ of the flow can also increase the stability, but to a much less extent than velocity.

For laminar flow the critical value of the stability criterion, $\theta_c = 1/Re^{1/3}$. This relationship was derived empirically from experimental results and generally indicates that mixing will occur in laminar flow when flow is at critical depth i.e. Fr = 1 (Vanoni, 1973). For turbulent flow, $\theta_c = 0.18$. In general, if θ is less than or equal to θ_c, mixing will occur at the interface (Vanoni, 1973, Middleton, 1966). However, if θ is greater than θ_c, the interface is stable and interfacial mixing is negligible.

The critical velocity at which mixing will occur across the interface can be determined by solving Eq. 18 for velocity and substituting θ_c for θ

$$V_c = \frac{(\nu g \Delta\rho/\rho)^{1/3}}{\theta_c} \qquad \cdots \cdots \cdots \cdots \cdots \cdots \cdots \quad (19)$$

θ can also be evaluated with regard to the Froude number. If the Froude number is equal to or greater than unity, the interface will be unstable. The higher the Froude number, the larger the amount of mixing across the interfacial boundary and entrainment of ambient water into the density current.

ROLE OF BUOYANCY

The density difference between the density current and the ambient water can be considered the buoyancy of the density current. Underflow density currents have a negative buoyancy. Buoyancy plays an important role in controlling the characteristics of the underflow. The driving force causing a density current to flow down an inclined slope is governed by the density difference and the slope angle. For a given slope, the greater the density difference, the larger the velocity of the flow (Eq. 12). Velocity is generally the controlling factor regarding whether a flow is laminar or turbulent as defined by the Reynolds number (Eq. 7). If the Reynolds number critical value of order 10^3 is reached, turbulent flow near the bed is expected. It has been shown that an increase in velocity, will also tend to decrease the stability of the current at the interface (Eq. 18).

The stability of the interface is also increased with an increase in the density difference (Eq. 18). For density current systems with relatively large density differences between the underflow and ambient water and small interfacial shears, turbulence at the interface will be damped out and appear laminar (Alavian et al. 1992). This is assuming the critical velocity (Eq. 19) with regard to stability has not been reached.

The density difference governing a density current controls the stability of the underflow along the incline and at the interfacial boundary. A large density difference can cause acceleration and destabilization of flow along the incline and damping and stabilization at the interfacial boundary.

PREDICTIONS OF DENSITY CURRENT CHARACTERISTICS

Based on the analysis of density current flow presented previously, predictions will be made regarding the characteristics of density current flow which will be conducted in an experimental flume. For purposes of this discussion, saline (NaCl) density currents will be considered because the kinematic viscosities for various concentrations are readily available in tables. Additionally, the buoyancy flux for saline density currents can be considered constant, whereas density currents consisting of suspended-sediments have a constant buoyancy flux only if the amount of sediment in the current remains constant. Deposition or erosion (entrainment) of bed material by a suspended sediment density current will cause the buoyancy flux to vary.

The flume will consist of an inclined bottom and channel submerged below fresh water. The density current will be introduced below the water surface to the head of the channel. The channel will be approximately 1 cm wide and approximately 4 cm deep, and the slope of the channel for various experimental runs will be 0.005, 0.05, 0.25, and 0.55. All runs will have laminar flow with Reynolds numbers between 8 and 100. The density of the underflow for various runs will be 1.05, 1.1, 1.15, and 1.2 g/cm^3.

Example Predictions

An underflow density current with a density of 1.10 g/cm^3 and a kinematic viscosity of 1.196 cS is introduced into the channel. The flow depth is 2 cm. The predicted characteristics of the flow can be determined as follows:

$$V = \sqrt{8(\Delta\rho/\rho)g/f_o(1 + \alpha)} \sqrt{dS}$$

$$= \sqrt{(8((1.10 - 1.0)/1.10))980) /(0.88(1.64))} \sqrt{(2)(0.55)}$$

$$= 23.3 \text{ cm/s}$$

$$Re = Vd/\nu = (23.3 \text{ cm/s})2 \text{ cm}/1.196 \text{ cS} = 39$$

$$Fr = V/(g'd)^{1/2} = (23.3 \text{ cm/s})/((89 \text{ cm/s}^2)2 \text{ cm})^{1/2} = 1.7$$

The density current flow would be laminar and supercritical. The predicted interfacial stability of the flow can be determined by

$$\theta = (\nu g \Delta\rho/\rho)^{1/3}/V = 1/(Fr^2 Re)^{1/3}$$

$$= 1/[(1.7^2)39]^{1/3}$$

$$= 0.21$$

Since the flow is laminar,

$$\theta_c = 1/Re^{1/3} = 1/39^{1/3}$$

$$= 0.29$$

For this flow $\theta < \theta_c$, so the interface is unstable and some mixing will occur.

The critical velocity at which the interface would become unstable under these flow conditions can be predicted by

$$V_c = (\nu g \Delta\rho/\rho)^{1/3}/\theta_c$$

$$= [(1.196 \ cS)980 \ cm/s^2(0.1/1.1)]^{1/3}/0.29$$

$$= 16.3 \ cm/s$$

Therefore, if the density current velocity is less than 16.3 cm/s, the interface should be stable with negligible mixing.

Effects of Slope

Variations in the density current velocity, depth, Froude number, and stability parameter for four different slopes are presented in Table 1. The density, kinematic viscosity, and Reynolds number are the same as for the example above, and remain constant for each slope setting.

TABLE 1
SALINE DENSITY CURRENT
FLOW CHARACTERISTICS WITH VARIATIONS IN SLOPE

S	V (cm/s)	d (cm)	Fr	θ	θ_c
0.005	4.9	9.7	0.2	0.95	0.29
0.05	10.6	4.5	0.5	0.44	0.29
0.25	18.2	2.6	1.2	0.26	0.29
0.55	23.6	2.0	1.7	0.20	0.29

Constant Re = 40; f = 0.884; ν = 1.196 cS; and ρ = 1.1 g/cm^3

The velocity and Froude number for the density current flow increase with each increase in slope. The flow depth and stability parameter decrease with increase slope. For the slope of 0.25, the Froude number is 1.2 and θ = 0.26 and θ_c = 0.29, indicating that the interface is unstable under these flow conditions.

Effects of Density

Variations in the density current flow characteristics for various densities are summarized in Table 2. The slope (0.55), density of ambient, and Reynolds number (100) were constant for each calculation. The kinematic viscosity is included in the table to illustrate how it increases with increased fluid density. The values were obtained from the Handbook of Chemistry and Physics.

TABLE 2
SALINE DENSITY CURRENT
FLOW CHARACTERISTICS WITH VARIATIONS IN DENSITY

ρ (g/cm³)	ν	V (cm/s)	d (cm)	Fr	θ
1.05	1.074	34.1	3.2	2.8	0.11
1.10	1.196	43.6	2.8	2.8	0.11
1.15	1.357	51.1	2.7	2.8	0.11
1.20	1.662	59.1	2.8	2.8	0.11

Constant Re = 100; f = 0.354; ρ_a = 1.0 g/cm³; and S = 0.55

The velocity of the density current increased with each increase in density. A 14 percent increase in density (from 1.05 to 1.2 g/cm³) resulted in a 73 percent increase in velocity (from 34.1 to 59.1 cm/s). The depth values fluctuated between 2.7 to 3.2 because the Reynolds number remained constant while the velocity and kinematic viscosity both increased with increased density.

Effects of Reynolds Number

The flow characteristics for variations in the Reynolds number are shown in Table 3. The slope (0.55), density (1.10 g/cm³), and kinematic viscosity (1.196 cS) are constant for each calculation.

The velocity, depth, and Froude number all decrease with a decrease in the Reynolds number as is expected. For this slope of 0.55, flow is supercritical for Reynolds numbers greater than approximately 15. To maintain subcritical density current flow under these flow conditions, the flow velocity will need to be no greater than approximately 10 cm/s.

TABLE 3
SALINE DENSITY CURRENT
FLOW CHARACTERISTICS WITH VARIATIONS IN REYNOLDS NUMBER

Re	f	d (cm)	V (cm/s)	Fr	θ	θ_c
100	0.35	2.8	43.6	2.8	0.11	0.22
80	0.44	2.6	37.5	2.5	0.13	0.23
60	0.59	2.3	31.0	2.1	0.15	0.26
40	0.88	2.0	23.6	1.7	0.20	0.29
20	1.77	1.6	14.9	1.2	0.32	0.37
10	3.54	1.3	9.3	0.9	0.50	0.47
8	4.42	1.2	8.1	0.8	0.58	0.50

Constant S = 0.55; ρ = 1.10 g/cm^3; and ν = 1.196 cS

CONCLUSIONS

The analysis presented in this paper indicates that steady, uniform density current flow can be characterized by a Chezy type equation. For laminar flow the Chezy type equation can be written as

$$V = \sqrt{8(\Delta\rho/\rho)g/f_o(1 + \alpha)}\,\sqrt{dS} = Re^{1/2}/2.7\,\sqrt{(\Delta\rho/\rho)gdS} \quad . \quad . \quad (17)$$

The analysis also indicates that the friction factor f is a function of the Reynolds number which for laminar flow can be expressed as

$$f = f_o(1 + \alpha) = 1.64f_o = 58/Re \quad . \quad . \quad . \quad . \quad . \quad . \quad . \quad . \quad . \quad . \quad . \quad (16)$$

The stability of the density current interfacial boundary is a function of the densimetric Froude number with the degree of instability and mixing increasing as the Froude number increases to values greater than unity. The critical value of the stability parameter occurs when the Froude number is unity.

The difference in density between the density current and ambient plays a dual role in determining the characteristics of the flow. High density differences promote greater flow velocities along an incline, as well as greater interfacial stabilities. Understanding how these two generally opposing forces interact and effect density current characteristics is important in understanding the dynamics of density currents.

APPENDIX I. - REFERENCES

Akiyama, J. and Stefan, H., 1985, Turbidity current with erosion and deposition, J. Hydr. Engrg., ASCE, Vol. 111, No.12, pp. 1473-1496.

Akiyama, J. and Stefan, H.G., 1987, Onset of underflow in slightly diverging channels, J. Hydr. Engrg., ASCE, Vol. 113, No. 7, pp. 825-844.

Alavian, V., 1992, Behavior of density currents on an incline, J. Hydr. Engrg., ASCE, Vol. 112, No. 1, pp. 27-42.

Alavian, V., Jirka, G.H., Denton, R.A., Johnson, M.C., and Stefan, H.G., 1992, Density currents entering lakes and reservoirs, J. Hydr. Engrg., ASCE, Vol. 118, No.11, pp. 1464-1489.

Ellison, T.H. and Turner, J.S., 1959, Turbulence entrainment in stratified flows, J. Fluid Mech., Vol. 6, pp. 423-448.

Garcia, M. and Parker, G., 1989, Experiments on hydraulic jumps in turbidity currents near a canyon-fan transition, Science, Vol. 245, pp. 393-396.

Guetter, A.K. and Jain, S.C., 1991, Analytical solution for density currents in settling basins, J. Hydr. Engrg., ASCE, Vol. 117, No. 3, pp. 324-345.

Harris, G.S., 1965, An inclined plume, J. Engrg. Mech. Div., ASCE, Vol. 91, No. EM1, pp. 7-18.

Komar, P.D., 1971, Hydraulic jumps in turbidity currents, G.S.A. Bull., Vol. 82, pp. 1477-1488.

Komar, P.D., 1972, Relative significance of head and body spill from a channelized turbidity current, G.S.A. Bull., Vol. 83, pp. 1151-1156.

Komar, P.D., 1977, Computer simulation of turbidity current flow and the study of deep-sea channels and fan sedimentation, The Sea, Vol. 6, pp. 603-621.

Kuenen, P.H., 1951, Properties of turbidity currents of high density, SEPM Special Pub. No. 2, pp. 14-33.

Kukushima, Y., Parker, G., and Pantin, H.M., 1985, Prediction of ignitive turbidity currents in Scripps submarine canyon, Marine Geology, Vol. 65, pp. 55-81.

Middleton, G.V., 1966, Experiments on density and turbidity currents: II. Uniform flow of density currents, Canadian J. of Earth Sci., Vol. 3, pp. 623-637.

Parker, G., Fukushima, Y., and Pantin, H.M., 1986, Self-accelerating turbidity currents, J. Fluid Mech., Vol. 171, pp. 145-181.

Vanoni, V.A., Editor, 1975, Sedimentation Engineering, ASCE Manual and Reports on Engineering Practice No. 54, pp. 278-285.

APPENDIX II. - NOTATION

B = buoyancy flux = $g'Vd$ = $g'Q$;
d = density current thickness;
f = total friction force = $f_0 + f_0$;
f_0 = friction force at channel;
f_i = friction force at interface;

g　　= gravitational acceleration;

g'　　= reduced gravitational acceleration = $(\Delta\rho/\rho)g$;

h_0　= thickness of density current below maximum velocity;

h_1　= thickness of density current above maximum velocity;

Fr　= densimetric Froude number = $V/(g'd)^{1/2}$;

Re　= Reynolds number = Vd/ν;

S　　= bottom slope;

V　　= mean velocity of density current;

α　　= interfacial shear stress constant = $[1 - 2(y_m/d)]/[1 + 2(y_m/d)] = h_1/h_0$;

$\Delta\rho$　= density difference between density current and ambient = $\rho - \rho_a$;

θ　　= stability parameter;

ρ　　= density of density current;

ρ_a　= ambient density;

τ_b　= bottom shear stress;

τ_i　= interfacial shear stress.